TECHNICAL MEMORANDUM

252

Impact of a validated radiative transfer scheme, RRTM, on the ECMWF model climate and 10 day forecasts

J-J. Morcrette, S.A. Clough, E.J. Mlawer and M.J. Iacono

Research Department

March 1998

European Centre for Medium-Range Weather Forecasts
Europäisches Zentrum für mittelfristige Wettervorhersage
Centre européen pour les prévisions météorologiques à moyen

Impact of a validated radiative transfer scheme, RRTM, on the ECMWF model climate and 10-day forecasts

Jean-Jacques Morcrette, Shepard A. Clough**

Eli J. Mlawer*, and Michael J. Iacono*

E.C.M.W.F., Shinfield Park, Reading Berkshire RG2 9AX, United Kingdom

**visiting ECMWF from AER*, Inc.

* Atmospheric and Environmental Research, Inc., Cambridge, Ma 02139

Abstract

In order to study the role of a better representation of the longwave radiation fluxes and cooling rates, the Rapid Radiative Transfer Model (RRTM: Mlawer et al., 1997) is introduced in the ECMWF model, and we perform a series of integrations with the cycle 16r2 version of the model including either RRTM or the operational longwave radiation scheme. Long-term response of the model is studied in T63 L31 4-month simulations for summer 1987 (MJJA) and winter 1987-88 (NDJF) whereas the impact on forecasts is discussed from a series of 12 T213 L31 experiments for the 15th of each month between April 1996 and March 1997.

In the chosen configuration for the ECMWF model which uses the diffusivity factor approximation to deal with the angular integration, RRTM is as efficient as the operational scheme for a 40-layer vertical resolution and much more efficient at higher resolutions. In clear-sky, RRTM corrects a number of systematic errors of the operational scheme, namely the excessive OLR and the underestimated surface downward radiation. The increased atmospheric opacity leads to a larger (reduced) radiative cooling rate in the higher (lower) troposphere. The absence of effective cloudiness approximation and the better spectral resolution of RRTM (16 vs. 6 spectral intervals) allows for a better handling of the radiative impact of clouds. The better spectral resolution is also important for the spectral representation of the surface emissivity.

Overall, the impact of RRTM is a warming and drying of the lower troposphere and a cooling of the higher troposphere and stratosphere. A decrease of cloudiness follows at most heights and latitudes together with an increase in surface skin temperature. The lower tropospheric warming leads to a decrease of the turbulent heat fluxes at most latitudes, but the decreased stability of the upper equatorial troposphere actually strengthens the Hadley circulation and converts large-scale precipitation into convective precipitation. A somewhat increased equator-pole temperature gradient increases the zonal mean wind in the winter hemisphere, and the easterlies in the equatorial region.

Objective scores for 10-day forecasts (without assimilation) show a minimum impact on anomaly correlation of geopotential at 1000 and 500 hPa, and a large and usually positive impact on the mean error of temperature at 850 and 200 hPa.

1. Introduction

The longwave (LW) radiation scheme, presently operational at ECMWF, is a band emissivity-type scheme. Transmissivities for H_2O and CO_2 , and their dependence on temperature were derived (Morcrette et al., 1986) from transmission functions computed with a narrow-band model (Morcrette and Fouquart, 1985). At the time of its development, this scheme was validated through comparison of fluxes and cooling rates computed with the Laboratoire de Meteorologie Dynamique (LMD) line-by-line model (Scott and Chedin, 1984). Since then, its absorption coefficients have been regularly updated following the availability of newer versions of the database of spectroscopic parameters (from HITRAN'82 to HITRAN'86 to HITRAN'92 to HAWKS'96). However the availability of schemes based on more efficient solutions of the radiative transfer equation, and of schemes validated not only on line-by-line model results, but also on actual spectrally detailed measurements makes it timely to reconsider the way the longwave radiation transfer is handled in the ECMWF model. Recently, such a scheme, the Rapid Radiative Transfer Model developed at the Atmospheric and Environmental Research, Inc. (AER RRTM) has been made available to ECMWF and thoroughly tested in both long integrations and 10-day forecasts. This paper reports the results of the various tests involved in this comparison.

2. Description of the radiation schemes

The AER RRTM longwave (LW) radiation code is described in detail in Mlawer et al. (1997). Here we concentrate on the aspects that differ most from the ECMWF operational LW scheme.

The operational LW scheme (Morcrette, 1988, 1991; see also ECMWF Model Documentation) accounts for absorption by water vapour, carbon dioxide, ozone, CH_4 , N_2O , CFC-11, and CFC-12. It is based on an emissivity method in which the transmission functions for water vapour and carbon dioxide over the six spectral intervals of the scheme have been fitted using Pade approximants on narrow-band transmissions obtained with statistical band models (Morcrette et al., 1986). At the time of its development, it was validated against the LMD 4A line-by-line model. However, some of its features make it somewhat outdated, particularly its parametrization of the water vapour continuum absorption, based on Roberts et al. (1976). In this scheme, semi-transparent clouds are treated using an effective cloud cover, the product of the actual cloud cover by the cloud emissivity.

As stated in Mlawer et al. (1997), the objective in the development of RRTM has been to obtain an accuracy in the calculation of fluxes and cooling rates consistent with the best line-by-line models. It utilizes the correlated-k method and shows its filiation to the AER line-by-line model (LBLRTM, Clough et al., 1989, 1992, Clough and Iacono, 1995) through its use of absorption coefficients for the relevant k-distributions derived from LBLRTM. Therefore the k-coefficients in RRTM include the effect of the CKD2.2 water vapour continuum (Clough et al., 1989). The accuracy of these absorption coefficients has been established by numerous and continuing high-resolution validations of LBLRTM with spectroscopic measurements, in particular those from the Atmospheric Radiation Measurement program (ARM). Compared to the original RRTM, the version used in this study has been slightly modified to account for cloud optical properties and surface emissivity defined for each of the 16 bands over which spectral fluxes are computed. Other changes are the use of a diffusivity approximation, instead of the 3-angle integration over the zenith angle, to derive upward and downward fluxes from the radiances, and the modification of the

original cloud random overlapping assumption to include (to the same degree of approximation as used in the operational SW scheme) a maximum-random overlapping of cloud layers.

For the relevant spectral intervals of both schemes, ice cloud optical properties are derived from Ebert and Curry (1992), and water cloud optical properties from Fouquart (1987), but whereas in the operational scheme the cloud emissivity used to compute the effective cloud cover is defined over the whole LW spectrum from spectrally averaged mass absorption coefficients and the relevant cloud water and/or ice paths (following Smith and Shi, 1992), in RRTM, the cloud optical thickness is defined as a function of spectrally varying mass absorption coefficients and relevant cloud water and ice paths, and is used within the true cloudy fraction of the layer.

Fluxes and cooling rates computed by RRTM and LBLRTM are compared in Mlawer et al. (1997). Here we compare fluxes and cooling rates from RRTM to those from the operational scheme. Figure 1 compares the upward and downward fluxes for the standard tropical, mid-latitude summer,

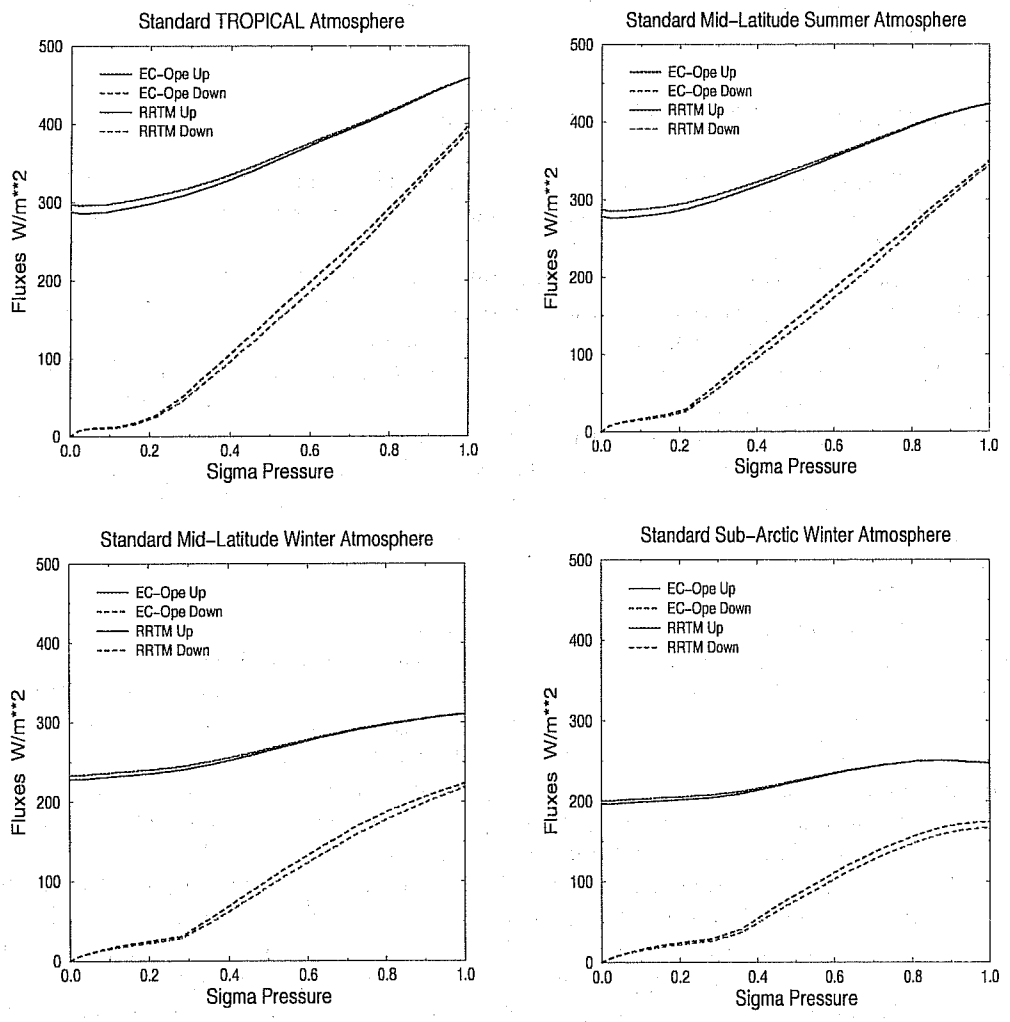

Figure 1: Comparison of RRTM and EC-Ope upward and downward fluxes.

mid-latitude winter, and sub-arctic winter atmospheres of McClatchey et al. (1972), whereas Figure 2 compares the corresponding cooling rates.

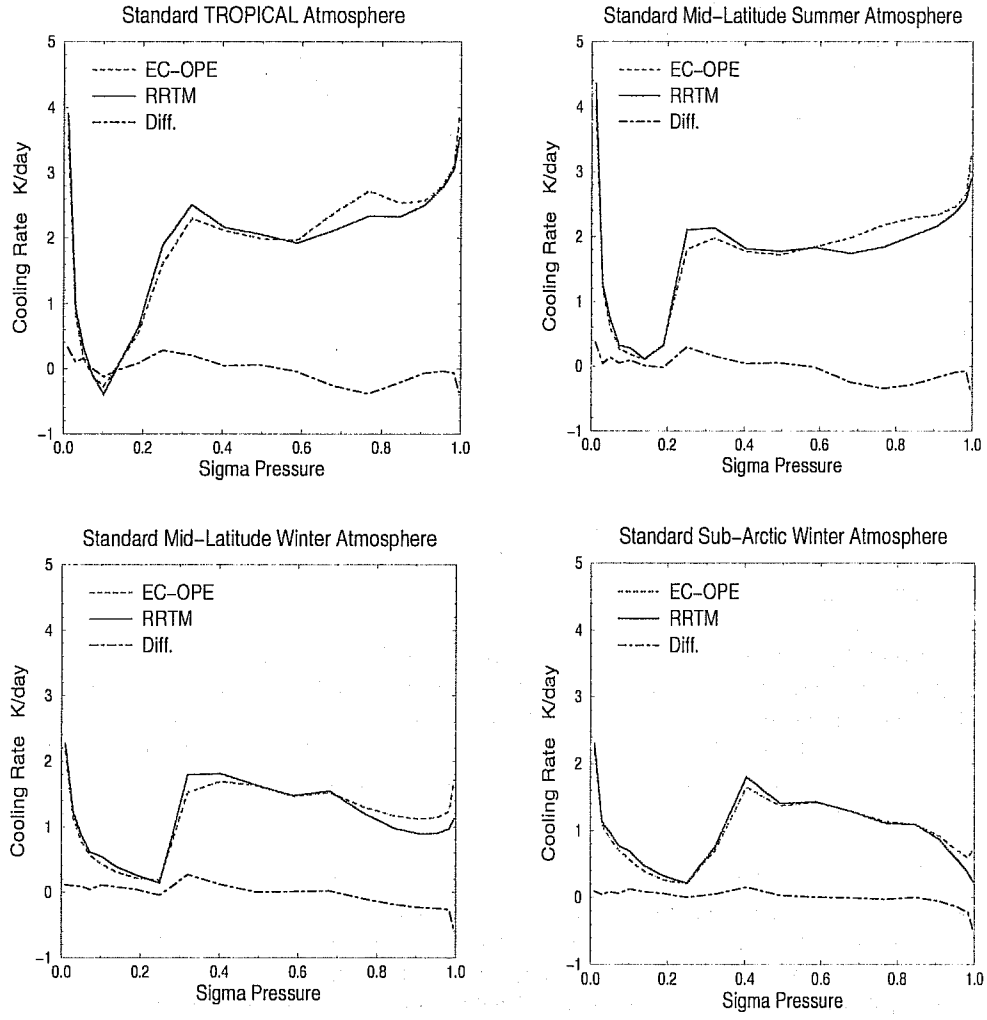

Figure 2: Comparison of RRTM and EC-OPE cooling rates (K/day).

The main difference between the two schemes is the increase in the intensity of the maximum cooling that RRTM brings to the clear-sky cooling rate for pressures between 200 and 400 hPa, and the decrease of the clear-sky cooling rate for pressures larger than 600 hPa, corresponding to an increase of the greenhouse effect of the longwave absorption, related to the improvement and strengthening of the water vapour p-type absorption, particularly important in the pure rotation part of the water vapour spectrum around 30 μm.

As RRTM is based on a two-stream solution of the LW radiation transfer, its efficiency depends linearly on the number of levels used to discretize the atmospheric profiles, whereas the operational

LW scheme, based on an emissivity method, includes a matrix solution of the radiative transfer and thus displays a quadratic dependence on the number of levels. The impact of this difference on the efficiency of the LW calculations is illustrated in Figure 3.

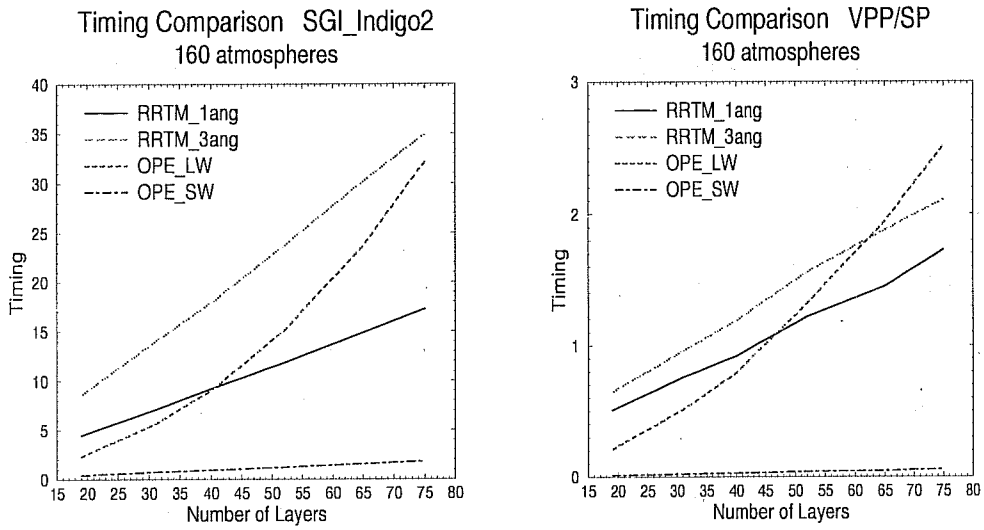

Figure 3: Timing comparison between the AER RRTM and the operational radiation schemes for a set of 160 31-level profiles run either on a SGI Indigo 2 workstation in scalar mode or on the VPP700 in vectorized mode.

In the course of the study, we tested various versions of RRTM. The original version (RRTM_3ang) handles the integration over zenith angle to go from upward and downward radiances to fluxes by explicitly integrating over three zenith angles. In the version used in the following comparison, we replace this integration by the diffusivity factor approximation (RRTM_1ang), thus allowing to make RRTM more computer efficient while retaining most of its accuracy (differences smaller than 0.5 W/m^2 on fluxes at the boundaries).

Inasmuch as RRTM computes total fluxes by integrating over 16 different spectral bands whereas the operational LW scheme considers 6 bands only, it is thus possible to improve on the spectral description of the surface or cloud radiative properties. For this report, we only studied the effect of improving the spectral description of the cloud optical properties, and recomputed the relevant cloud optical coefficients over the 16 bands of RRTM. This is a marked improvement over the longwave cloud emissivity approach (based on Stephens, 1978) used in the operational scheme, which considers the radiative effect of clouds only via an effective cloud cover, i.e., the product of the layer cloud fraction by an emissivity valid over the whole longwave spectrum.

3. Results of seasonal simulations

The impact of RRTM in the ECMWF model has been studied from two points of view, in terms of the modifications to the model systematic errors, through comparisons of T63 L31 summer 1987 (MJJA) and winter 1987-88 (NDJF) simulations, and in terms of potential improvements to the forecasts, through comparisons of objective scores for a series of twelve T213 L31 forecasts for the

15th of each month between April 1996 and March 1997. All following results have been obtained with the cycle 16r2 version of the model, which includes for the shortwave radiation transfer the scheme based on Fouquart and Bonnel (1980) (Morcrette, 1991, 1993).

For each of the seasonal runs, six simulations were performed, starting 24 hours apart from 26 April to 1 May and finishing on 1 September 1987, and from 27 October to 1 November and finishing on 1 March 1988. Such ensembles of experiments have been shown by Brankovic et al. (1994) to be large enough to give a reasonable level of statistical significance to the results of the comparison. In the following, results will concentrate on the summer experiments, but we obtain a similar impact of RRTM in the ECMWF model in the winter experiments. Most of the following results are presented for each individual set of six experiments, Control (or OPE) and RRTM, for the difference Control-RRTM (DIFF), and the statistical significance of the results is shown in terms of the Student's t-test (StT). Section 3.1 presents the initial forcing for the 1 May 1987, and section 3.2 discusses the three month averages for the the summer simulations. A small number of winter results are discussed in section 3.3.

3.1 Initial forcing

The effect of the increased longwave opacity of the atmosphere with RRTM is obviously present from the start of the model simulation, as can be seen from Figures 4 and 5, which show a comparison of the clear-sky outgoing longwave radiation and net longwave radiation at the surface during the first 24 hours of the simulations. The clear-sky OLR is decreased over most of the globe by quantities ranging from 2 Wm^2 at high latitudes to more than 8 Wm^2 in the equatorial region.

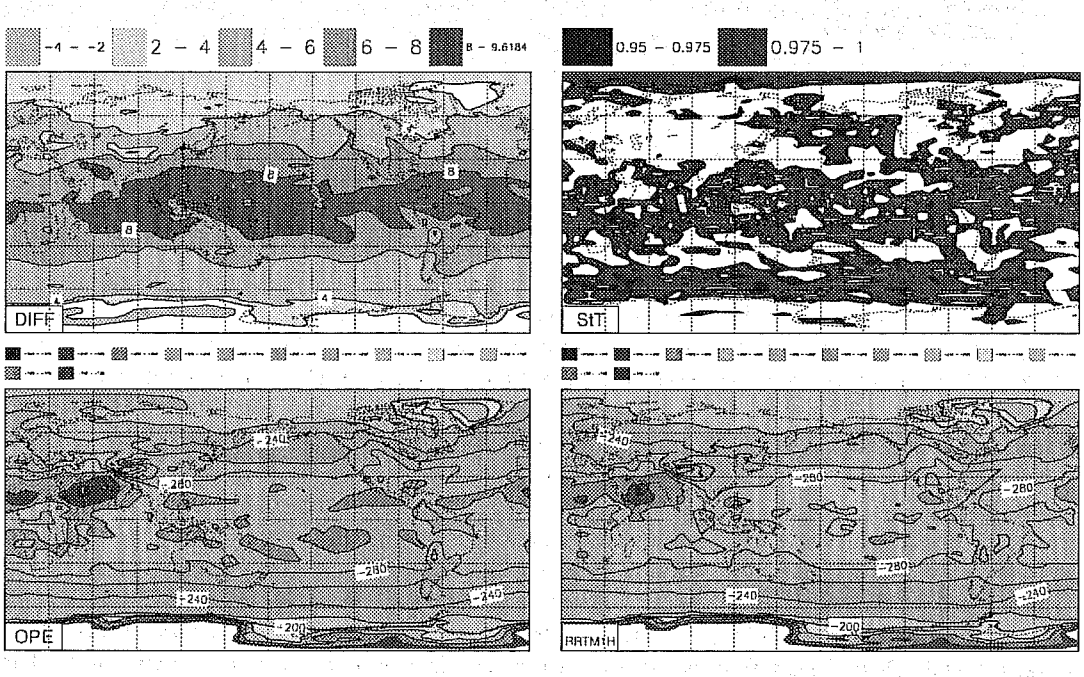

Figure 4: The clear-sky outgoing longwave radiation at the top of the atmosphere over the first 24 hours of integration. St is the result of the Student's T-test of statistical significance. Global means are: Control -270.7 W/m^2, RRTM -264.5 W/m^2, difference RRTM-Control 6.2 W/m^2.

The clear-sky net LW radiation at the surface (Fig. 5) is decreased due to the increase of the downward LW radiation, from less than 4 Wm^2 in the mid-latitudes to 6 Wm^2 in the tropics and more than 8 Wm^2 over the colder areas (Himalaya, Antarctica, Northern Canada).

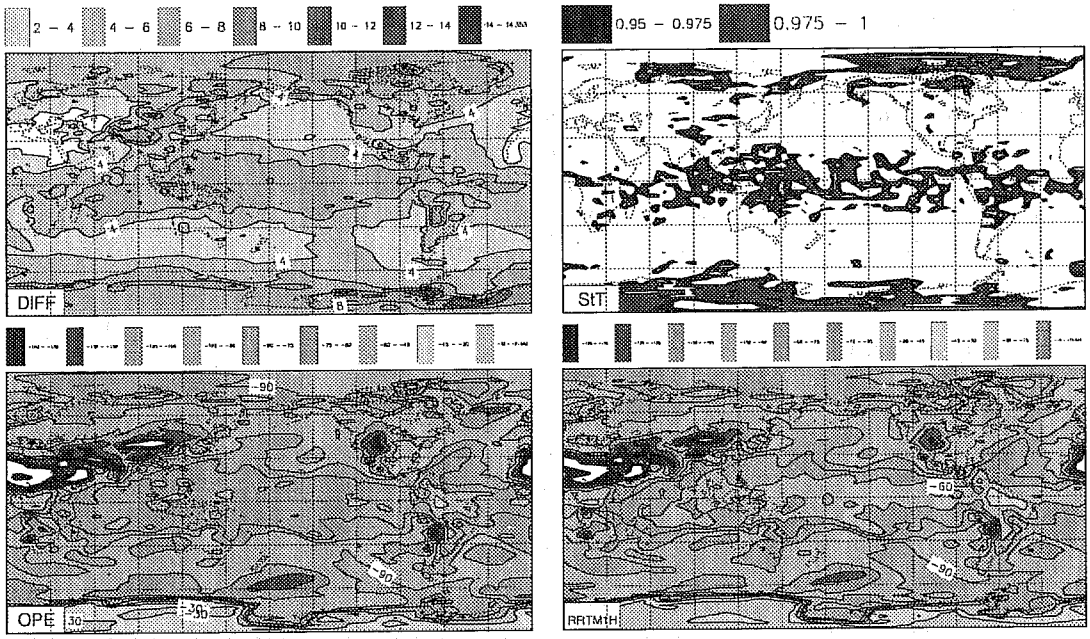

Figure 5: As in Figure 4, but for the clear-sky net longwave radiation at the surface. Global means are: Control -88.5 W/m^2, RRTM -83.6 W/m^2, difference RRTM-Control 4.9 W/m^2.

The initial impact of RRTM on the vertical distribution of the total LW cooling is shown in Figure 6. The change already noticed in one-dimensional clear-sky comparisons (increase of the cooling in high troposphere, decrease lower down) is further emphasized by the greenhouse effect of the clouds. The increased cooling amounts to more than 0.1 K/day in the high troposphere about 100 hPa below the tropopause (up to 1 K/day in the equatorial regionat 450 hPa) and a decreased cooling at heights below 650 hPa (up to 0.5 K/day in the sub-tropics). The effect of the better spectral description of the cloud band emissivity certainly adds up to the increased clear-sky greenhouse effect and decreases the cooling by the sub-tropical clouds. Figure 7 presents the initial impact on the total OLR. RRTM shows a marked decrease in OLR within the zonal band 40°N-40°S, but of much less statistical significance than the similar decrease in clear-sky OLR (Fig. 4). A similar effect of clouds appears also in Figure 8 for the total surface net LW radiation. This is linked to clouds having a variability equal to or higher than the signal of RRTM with respect to the operational scheme. Therefore the presence of clouds decreases the statistical significance of the changes brought by RRTM to the OLR and surface net LW radiation.

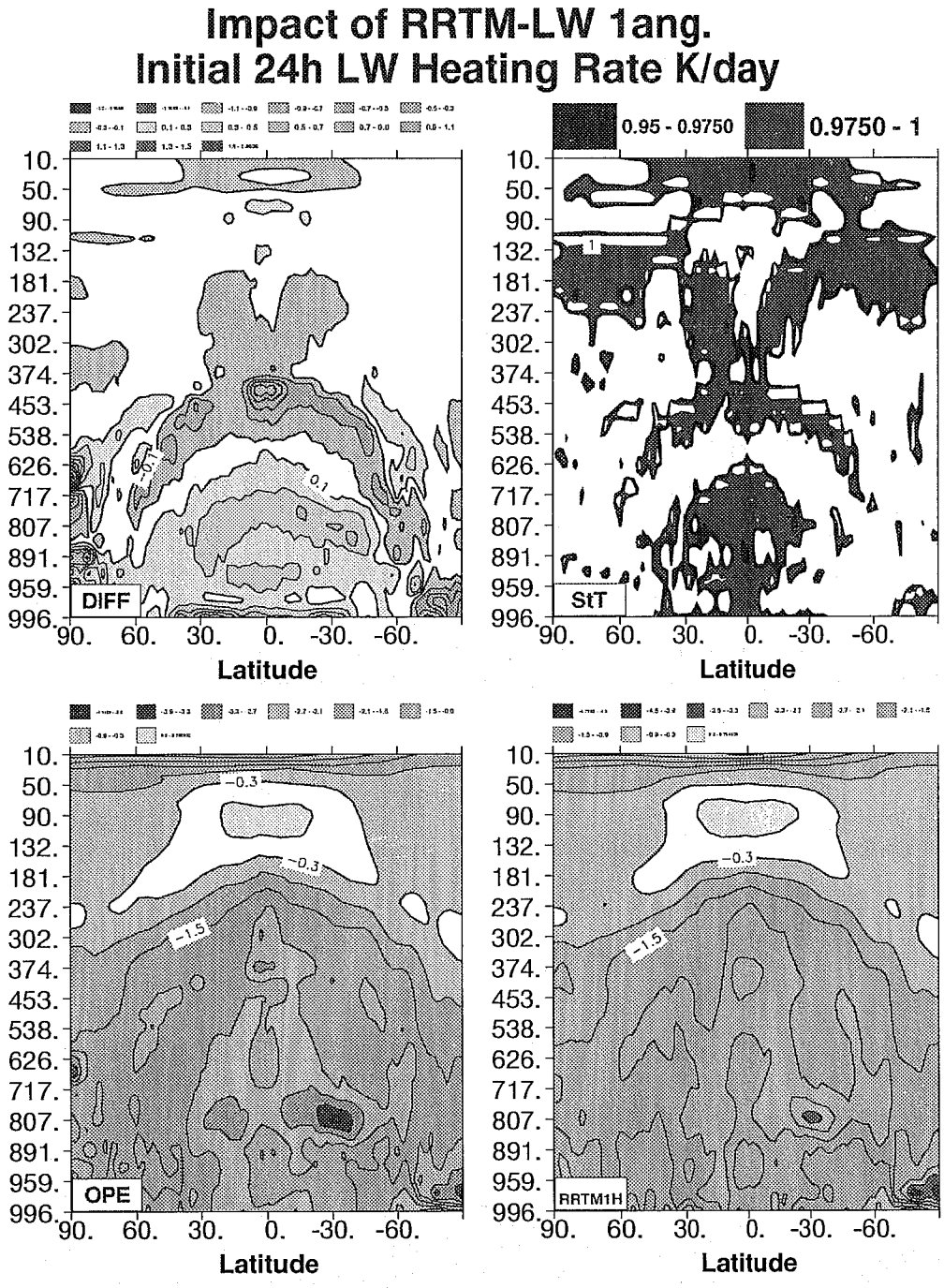

Figure 6: The vertical distribution of the zonally averaged longwave cooling rate over the first 24 hours of the sets of 6 integrations. Top left panel shows the difference RRTM-OPE (contour is 0.2 K/day starting from 0.1 K/day), top right is Student's t-test, bottom left is Control, bottom right panel RRTM. (contour is 0.6 K/day starting from 0.3 K/day).

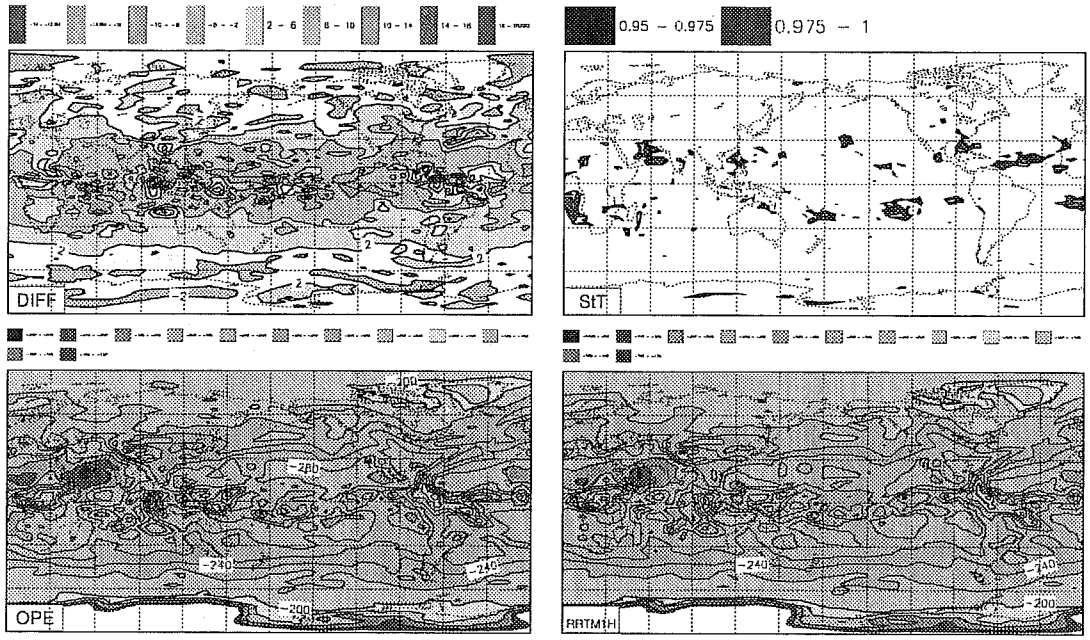

Figure 7: As in Figure 4, but for the total sky OLR at the top of the atmosphere. Global means are: Control -251.8 W/m^2, RRTM -247.8 W/m^2, difference RRTM-Control 4.1 W/m^2.

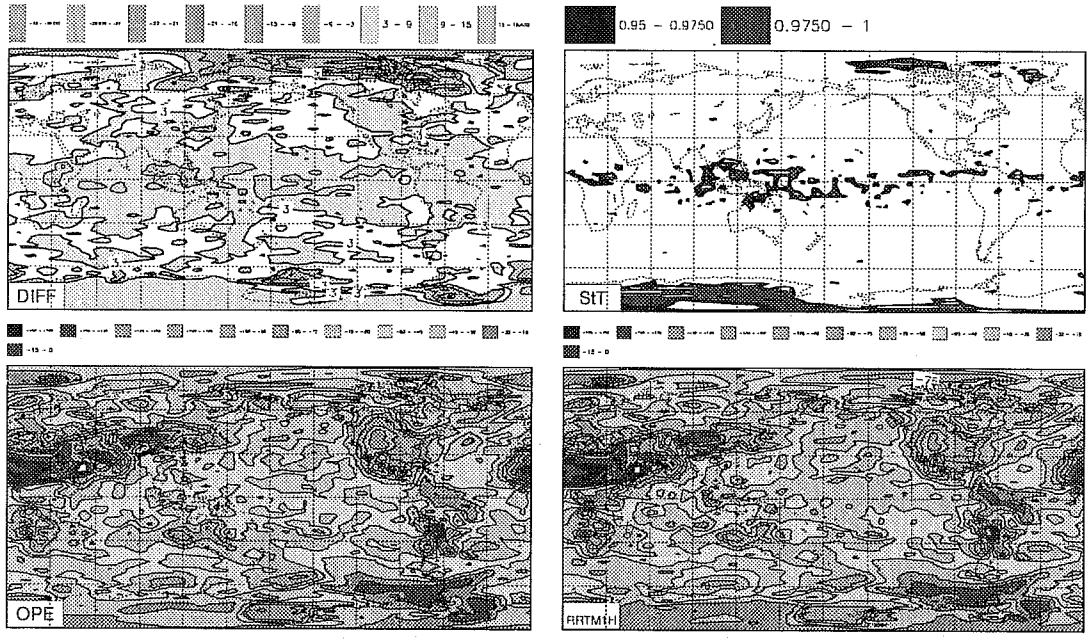

Figure 8: As in Figure 4, but for the total sky net longwave radiation at the surface. Global means are: Control -59.9 W/m^2, RRTM -56.6 W/m^2, difference RRTM-Control 3.3 W/m^2.

3.2 Three-month averages

In this section, the averages are computed over the last three months of the four month integration, namely between 870601 00Z and 870831 24Z. Results are again presented for each individual set of six experiments, Control (or OPE) and RRTM, for the difference RRTM-Control (DIFF), and the statistical significance of the results is shown in terms of the Student's t-test (StT). Physical fluxes are presented on the 31 vertical levels of the model, whereas the standard dynamical quantities (T, RH, winds, vertical velocity) are presented on the 15 standard fixed pressure levels.

For this three month average, the impact of RRTM is to decrease the clear-sky OLR by 6.3 Wm^2 (Fig. 9) and increase the clear-sky surface net LW radiation by 4.5 Wm^2 (Fig. 10). These signals are highly significant and encompass most latitudes of the globe. Similarly for cloudy fluxes, the OLR is decreased by 3.1 W/m^2 (Fig. 11), the surface net LW radiation by 2.4 W/m^2 (Fig. 12), and the signal, albeit of a smaller amplitude than during the initial 24 hours, because of adjustments in other variables, is significant over a larger fraction of the globe. These changes are also reflected in the vertical distribution of the radiative heating rates, themselves linked to various adjustments in the governing parameters of radiation, namely cloudiness, temperature and humidity fields. The pattern seen for the vertical distribution of the LW cooling rate during the initial 24 hours (Fig. 6) is maintained during the length of the simulation (Fig. 13). It is accompanied by an increase of the SW heating rate in the lower tropical troposphere and a decrease at higher levels in both the tropics and the summer hemisphere (Fig. 14). This can mainly be explained by the changes in cloudiness (Fig. 15: total cloudiness) where the high-, mid- and low-level cloudiness (Fig. 16, 17, and 18, respectively) decrease over most latitudes. Most of this decrease in clouds is statistically significant, the only exception being that of the low-level cloudiness. The reduction in mid-level cloudiness (Fig. 19) goes together with a similar reduction in cloud liquid water (Fig. 20). For the cloud ice water (CIW), the signal, as seen from zonal averages, is more complicated (Fig. 21): changes in CIW follow the changes in cloudiness lower down, but below the tropopause in the Northern hemisphere, an increase in CIW around 500 hPa and 60 ^oN is in fact associated with a decrease in cloudiness.

The overall reduction in cloudiness and cloud water loading accounts for the increase in absorbed SW radiation as seen from the top of the atmosphere (Fig. 22). Together with the increase in surface net LW radiation (Fig. 12), which is linked to the increased clear-sky LW opacity of RRTM, the reduced cloudiness also increases the surface net SW radiation (Fig.23) and thus the surface net total (LW+SW) radiation (not shown). As a result of the decreased LW cooling / increased SW heating in the layers close to the surface (Figs. 13 and 14), we can expect the latent (Fig. 24) and sensible heat flux (Fig. 25), whose intensities depend on the gradient between surface and lower model level values of, respectively, specific humidity and temperature, not to compensate completely the increase in surface net radiation, thus resulting in an overall increase in net heat flux at the surface (Fig. 26). This increase occurs over most of the oceans, with the notable exception of the Southern oceans where some positive/negative patterns in the South Pacific around 60 ^oS and continuing in the South Atlantic around 45 ^oS are seen in net LW radiation (Fig. 12), and latent and sensible heat fluxes (Figs. 24 and 25, respectively). These exceptions are linked to the pattern of the changes in low-level cloudiness (Fig. 18). A similar type of signal can also been seen in all fields over India.

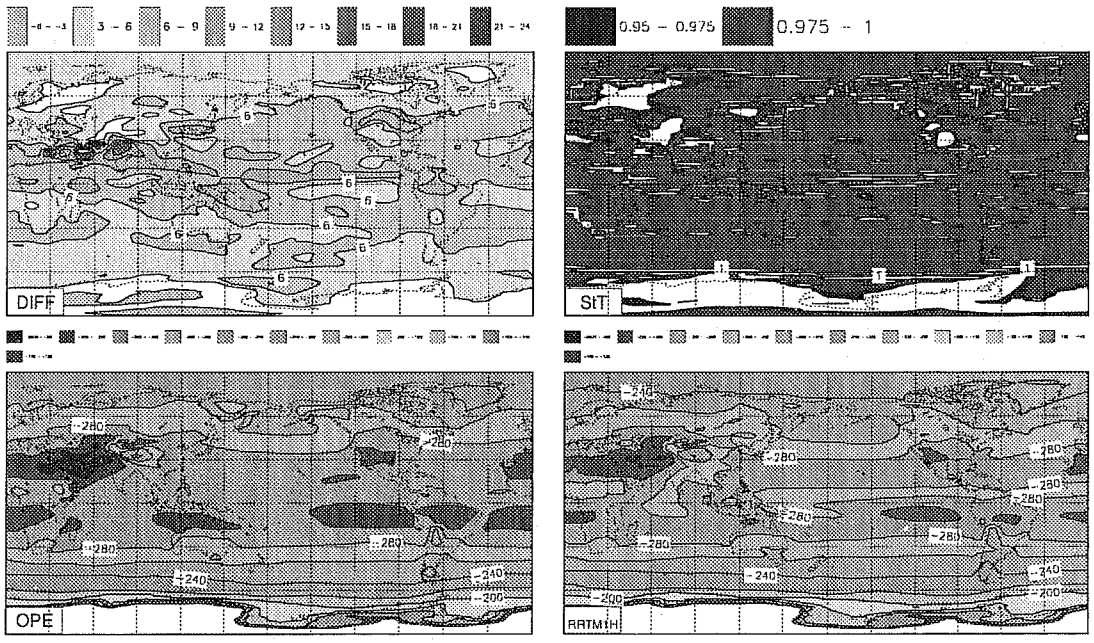

Figure 9: The clear-sky outgoing LW radiation at the top of the atmosphere averaged over 92 days between 870601 00Z and 870831 24Z. Global means are: Control -272.5 W/m^2, RRTM -266.2 W/m^2, difference RRTM-Control 6.3 W/m^2.

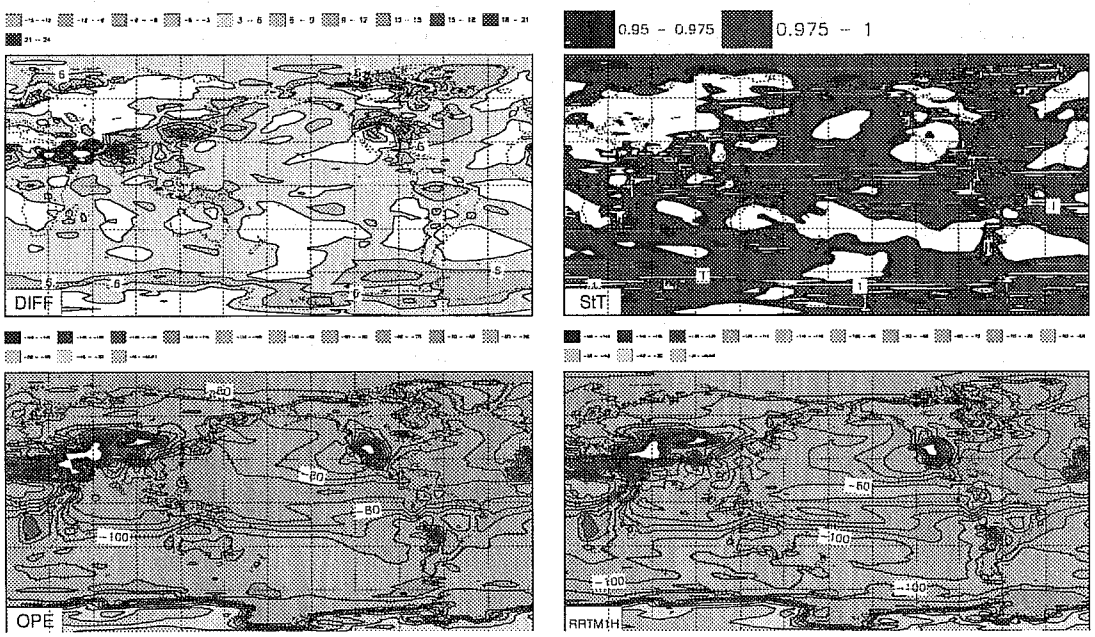

Figure 10: As in Figure 9, but for the clear-sky net LW radiation at the surface. Global means are: Control -89.1 W/m^2, RRTM -84.7 W/m^2, difference RRTM-Control 4.5 W/m^2.

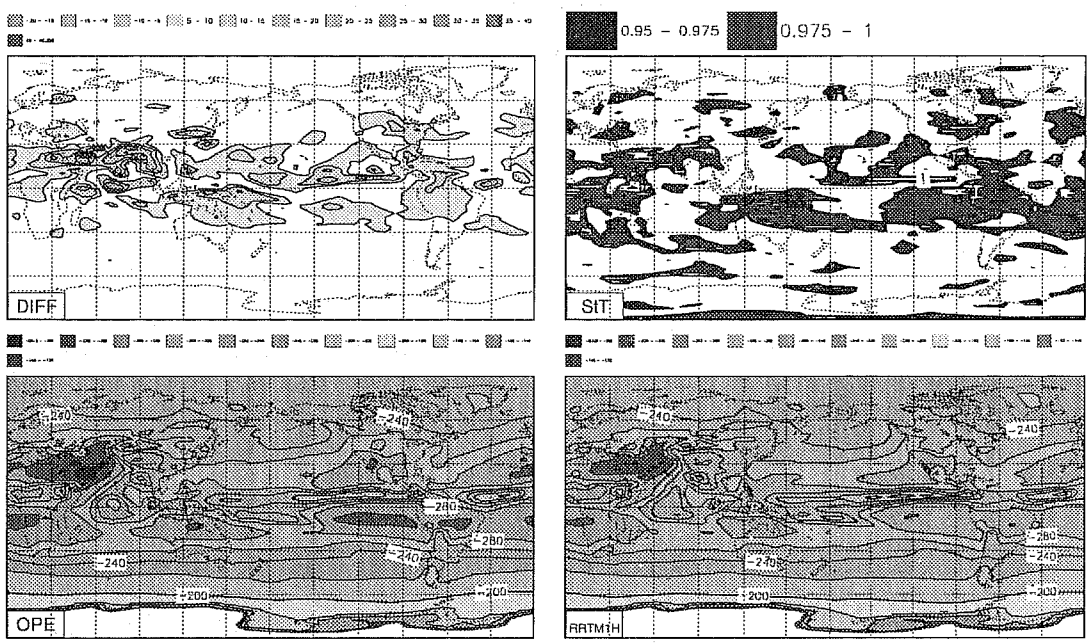

Figure 11: As in Figure 9, but for the total sky OLR. Global means are: Control -251.3 W/m^2, RRTM -248.2 W/m^2, difference RRTM-Control 3.1 W/m^2.

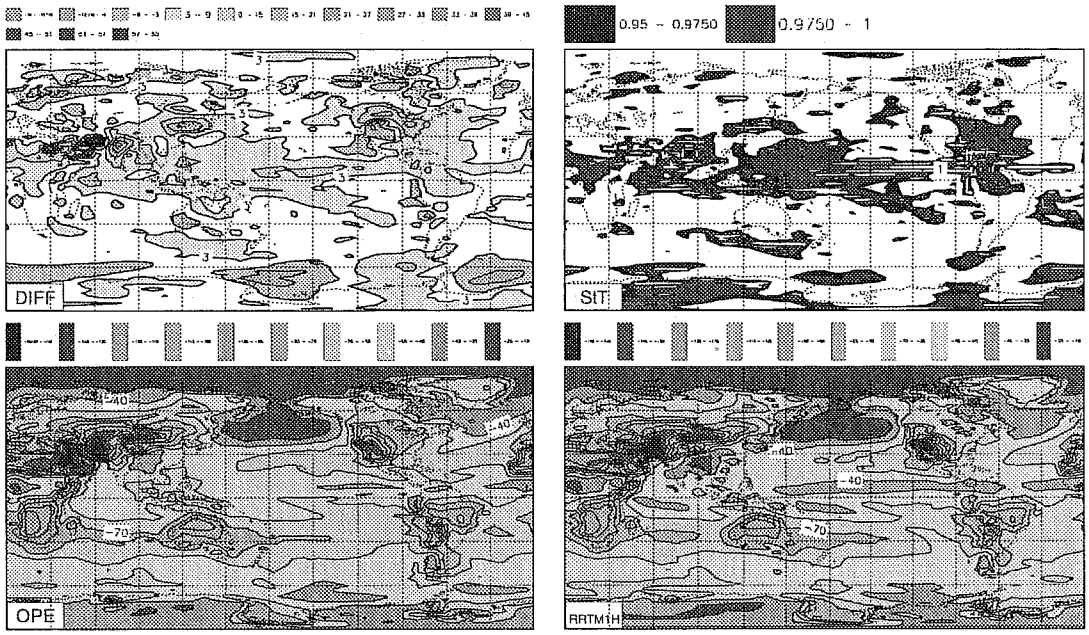

Figure 12: As in Figure 9, but for the total sky net LW radiation at the surface. Global means are: Control -59.2 W/m^2, RRTM -56.9 W/m^2, difference RRTM-Control 2.4 W/m^2.

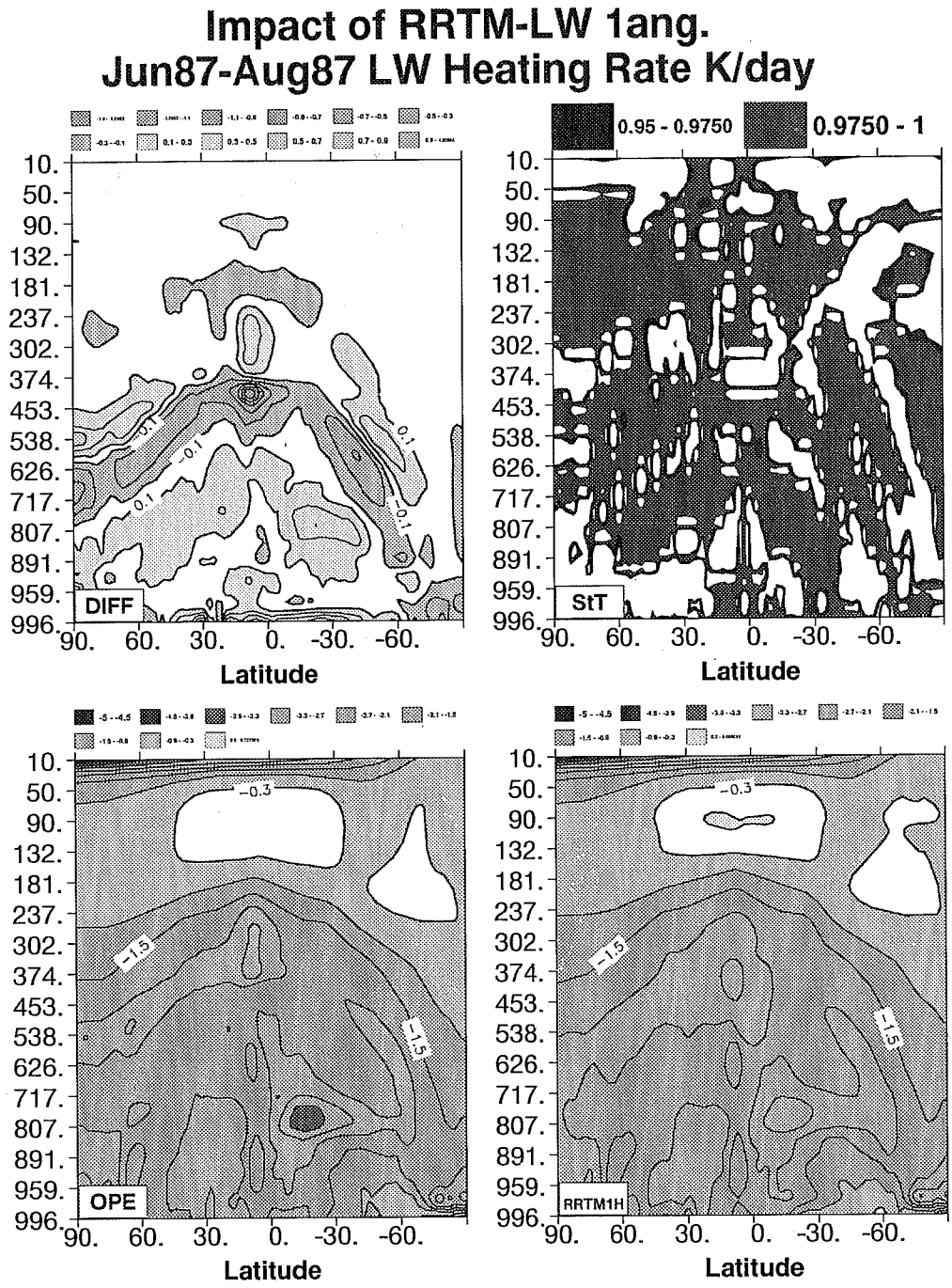

Figure 13: The vertical distribution of the zonal mean LW heating rate (K/day) averaged over JJA87.

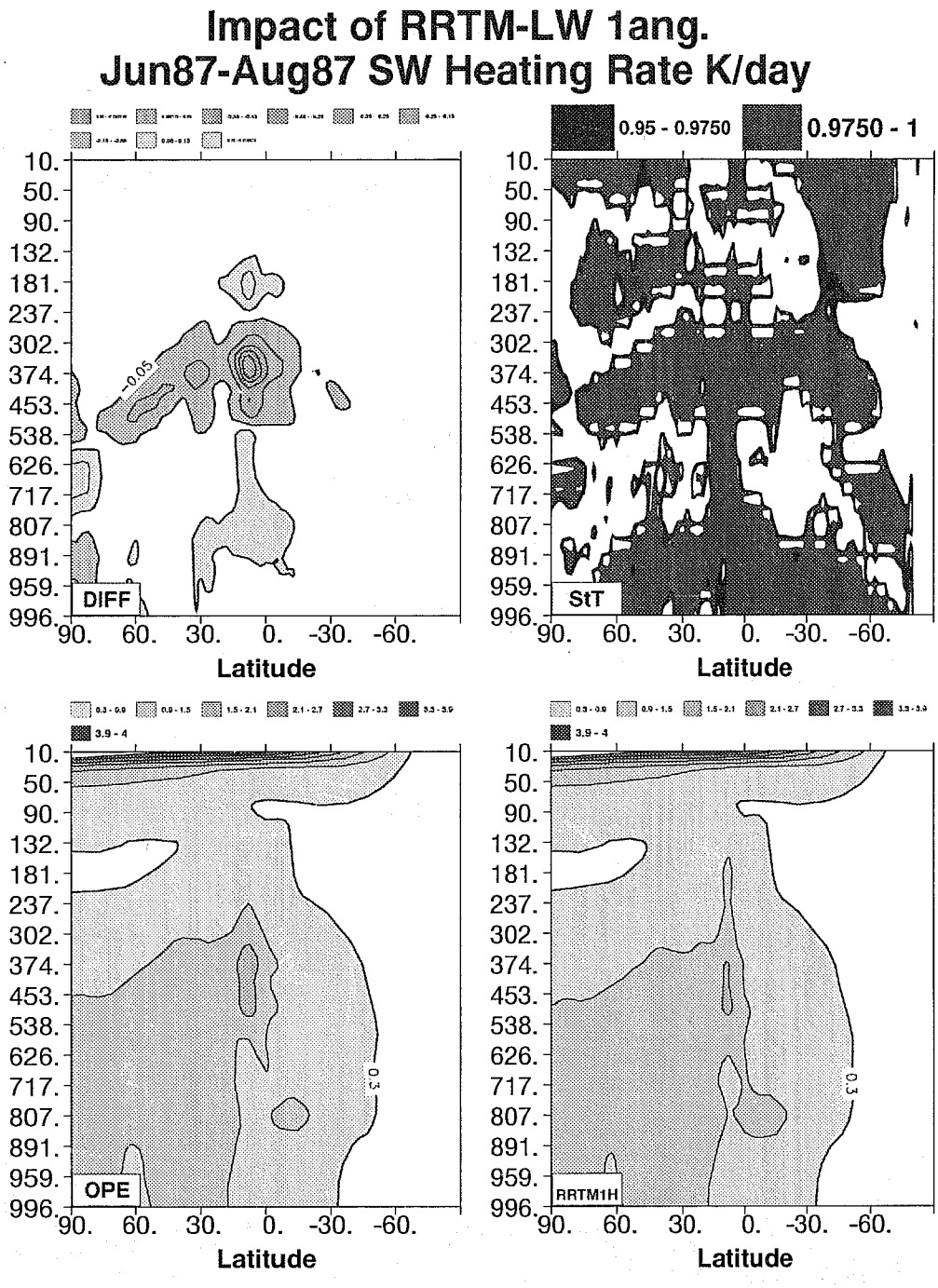

Figure 14: As in Figure 13, but for the SW heating rate (K/day).

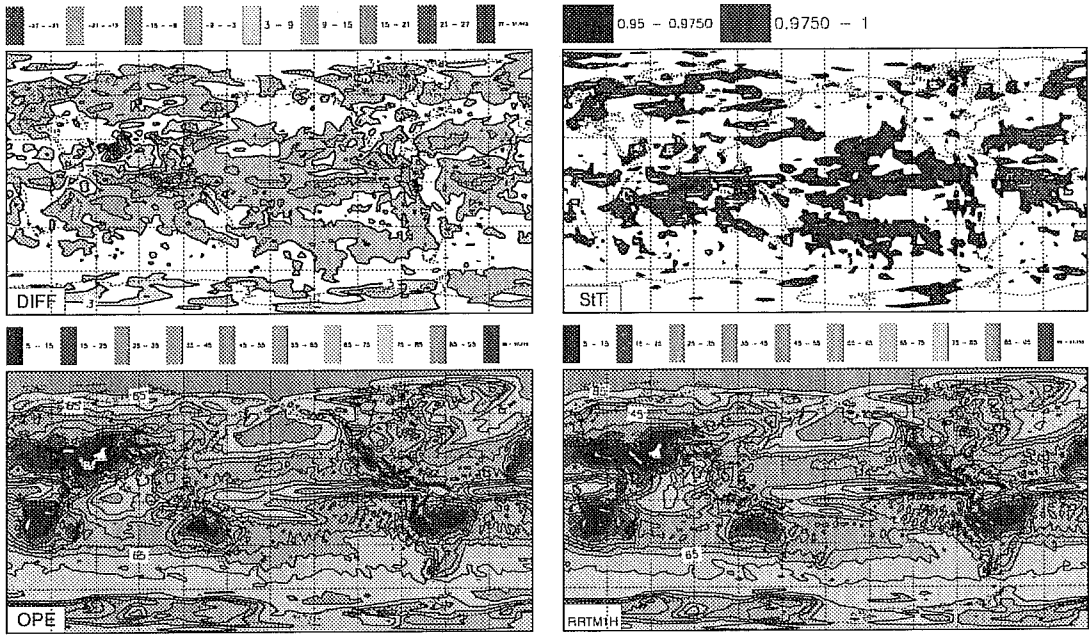

Figure 15: As in Figure 9, for the total cloudiness. Global means are: Control 57.2 %, RRTM 53.9 %, difference RRTM-Control -3.3 %.

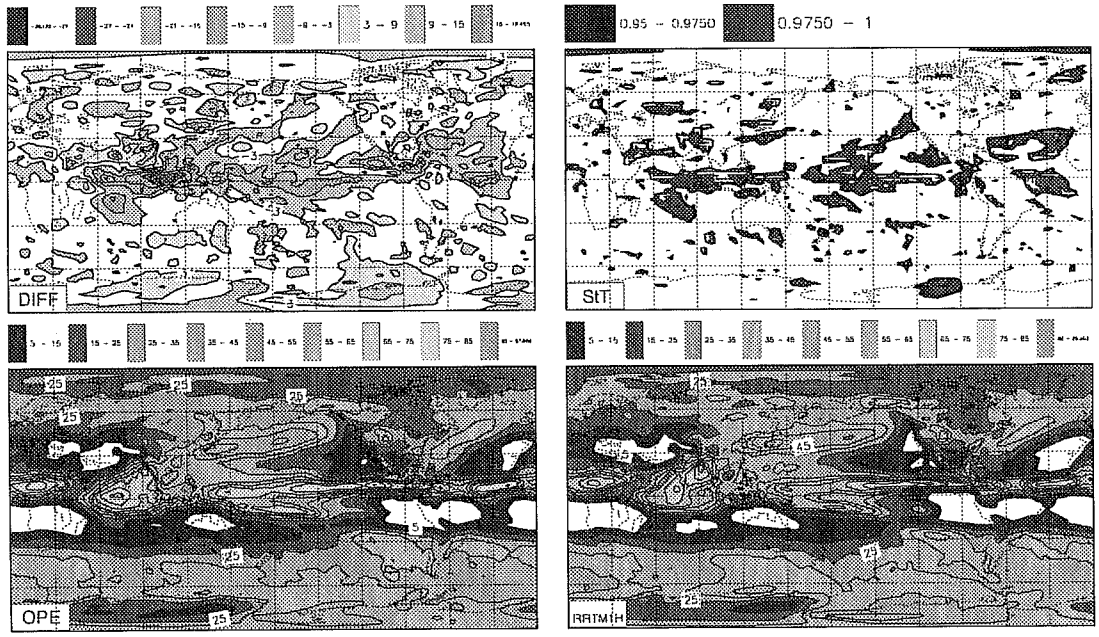

Figure 16: As in Figure 9, but for the high level cloud cover (above sigma=0.45). Global means are: Control 28.5 %, RRTM 26.8 %, difference RRTM-Control -1.7 %.

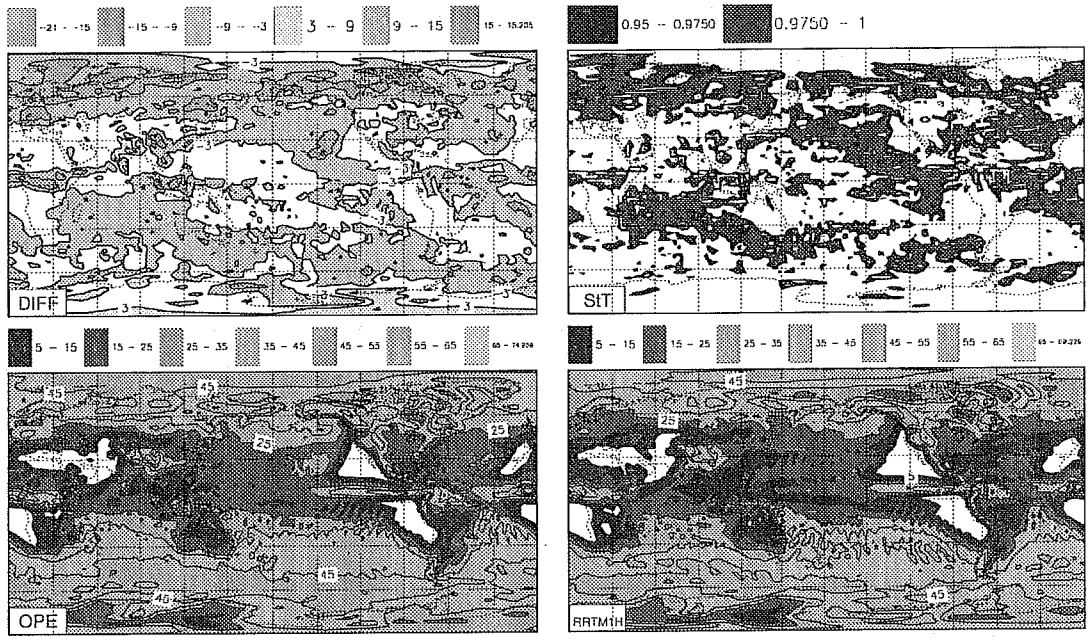

Figure 17: As in Figure 9, but for the middle level cloudiness ($0.80 < \sigma < 0.45$). Global means are: Control 28.0 %, RRTM 24.5 %, difference RRTM-Control -3.5 %.

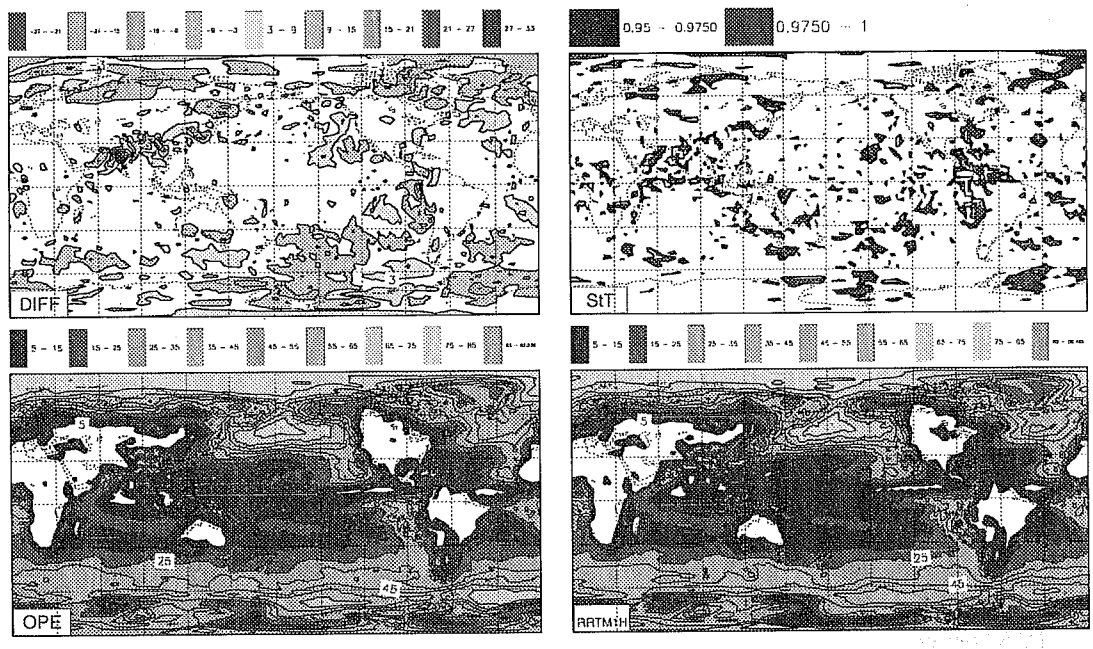

Figure 18: As in Figure 9, but for the low level cloudiness (sigma > 0.80). Global means are: Control 21.9 %, RRTM 21.4 %, difference RRTM-Control -0.5 %.

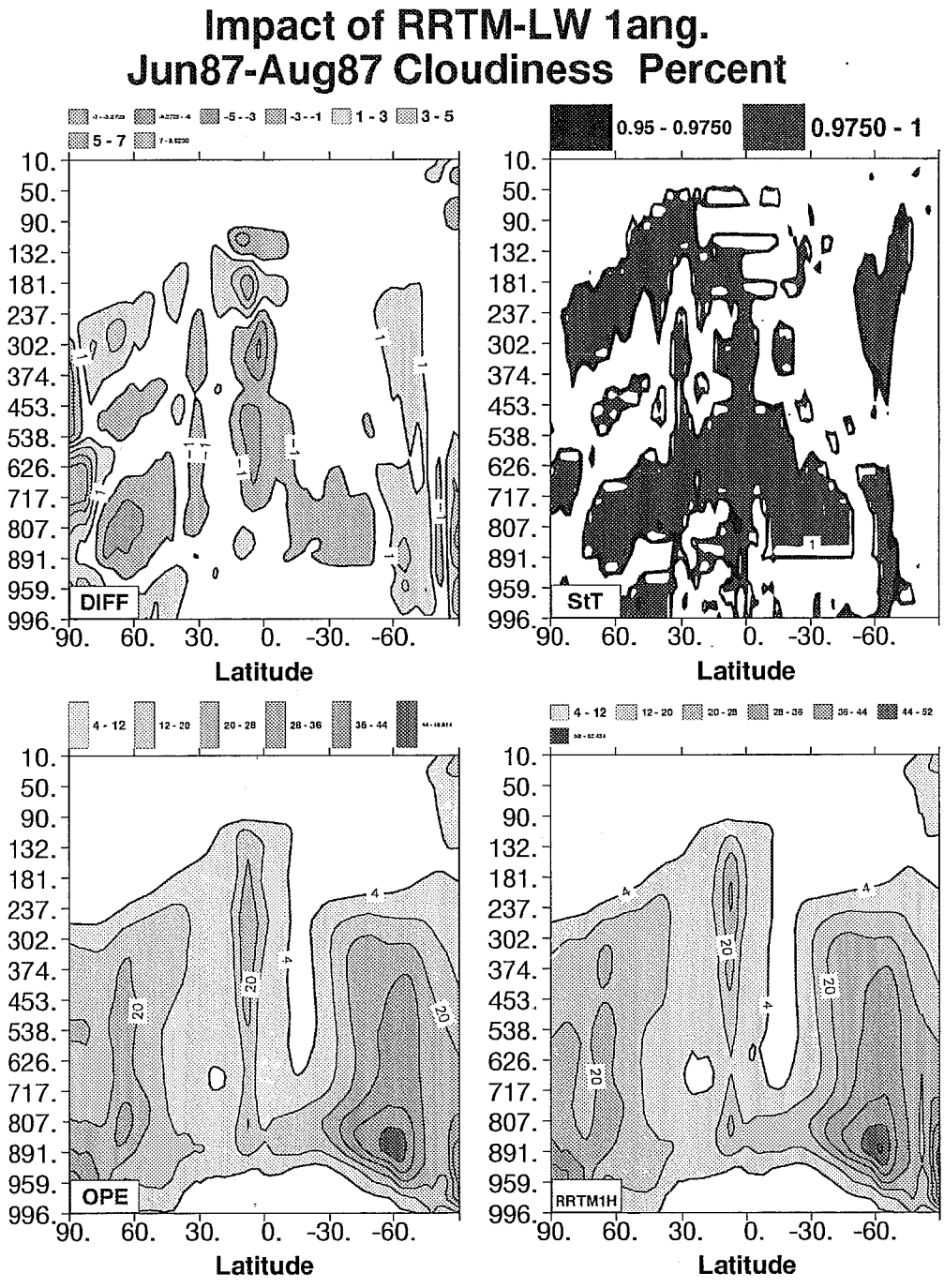

Figure 19: The vertical distribution of the zonal mean cloud fraction (percent) averaged over the JJA87 period.

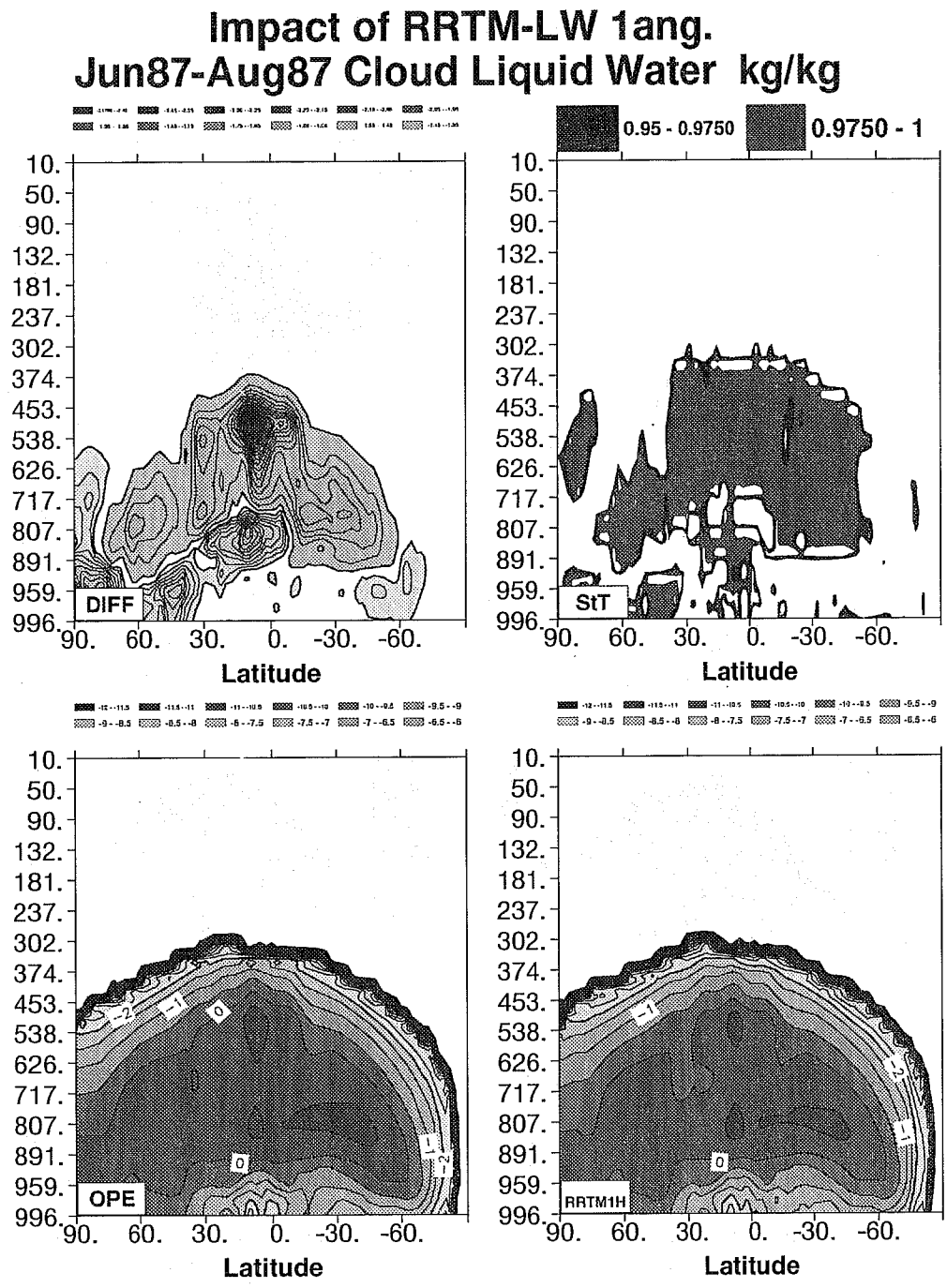

Figure 20: As in Figure 19, but for the cloud liquid water. Top left panel is the difference of CLW between RRTM and Control (positive contour is 0.02, negative contour is 0.05), wheras the bottom panels show $\log_{10}$ (CW).

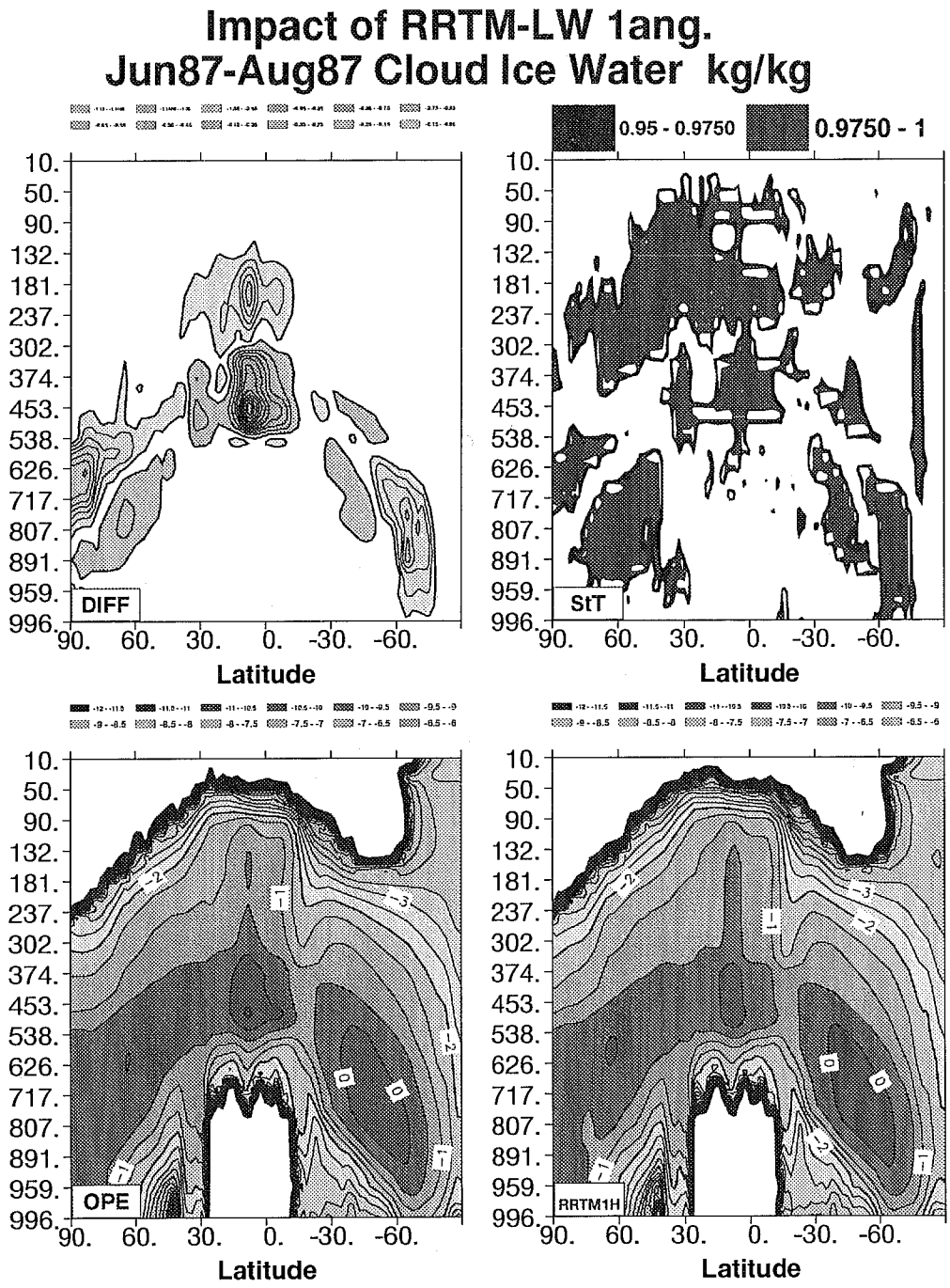

Figure 21: As in Figure 19, but for the cloud ice water. Same contours as in Figure 20.

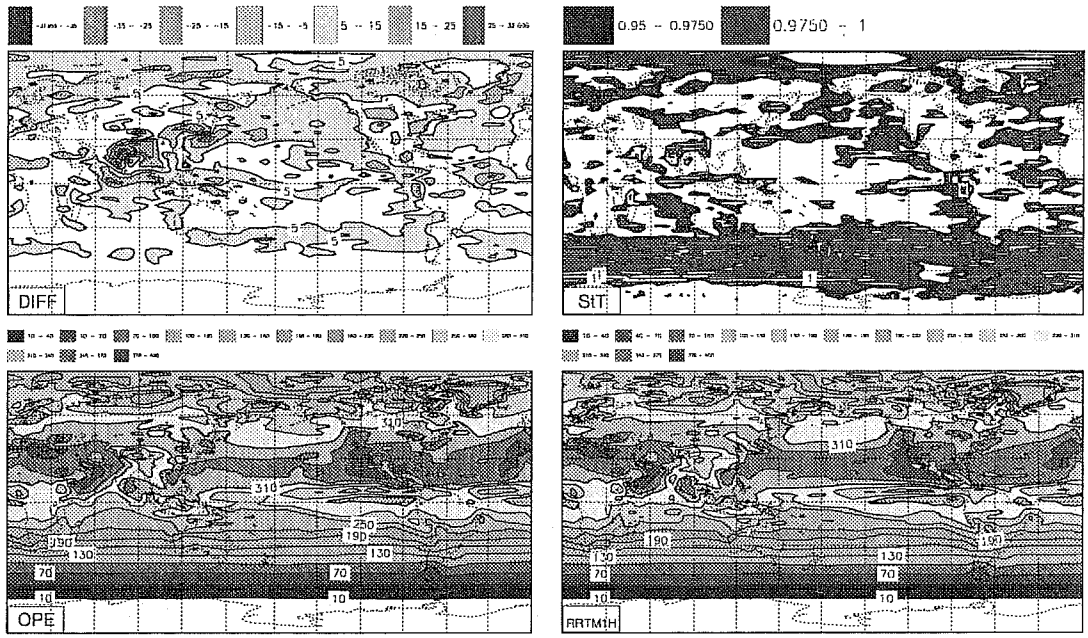

Figure 22: As in Figure 9, but for the total sky absorbed SW radiation at the top of the atmosphere. Global means are: Control 231.5 W/m^2, RRTM 235.2 W/m^2, RRTM-Control 3.7 W/m^2.

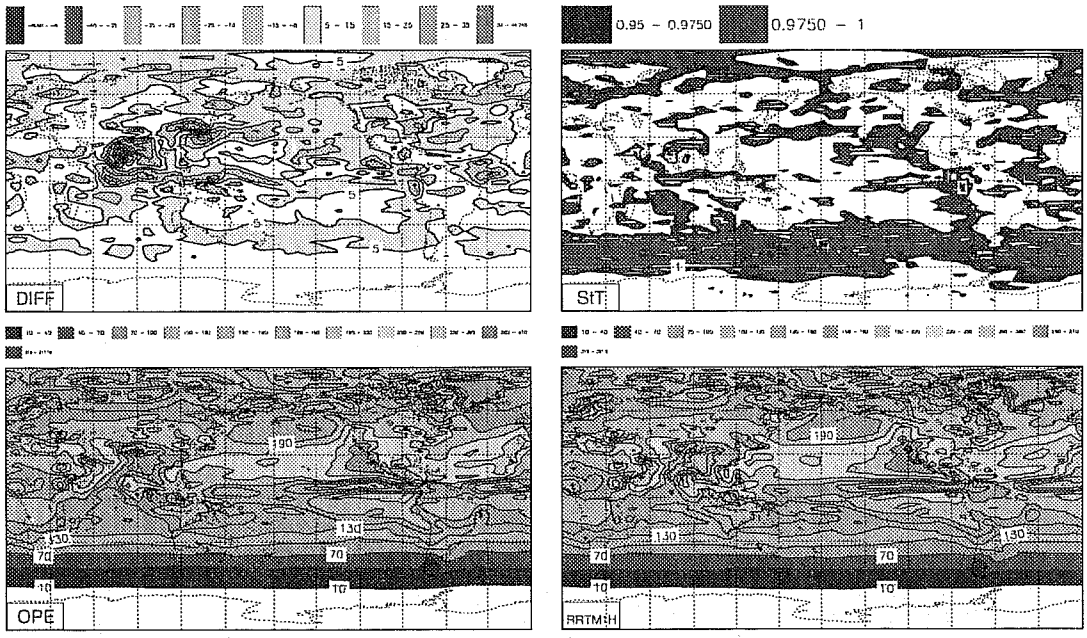

Figure 23: As Figure 9, but fot the total sky net SW radiation at the surface. Global means are: Control 147.3 W/m^2, RRTM 151.8 W/m^2, difference RRTM-Control 4.5 W/m^2.

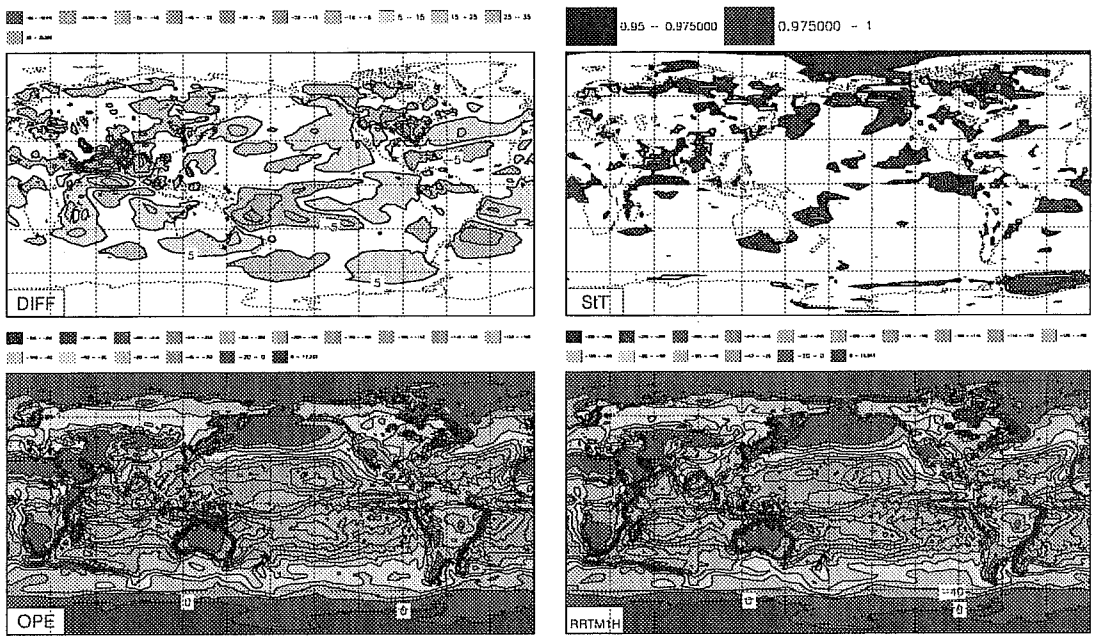

Figure 24: As in Figure 9, but for the surface latent heat flux. Global means are: Control -90.1 W/m^2, RRTM -90.4 W/m^2, difference RRTM-Control -0.3 W/m^2.

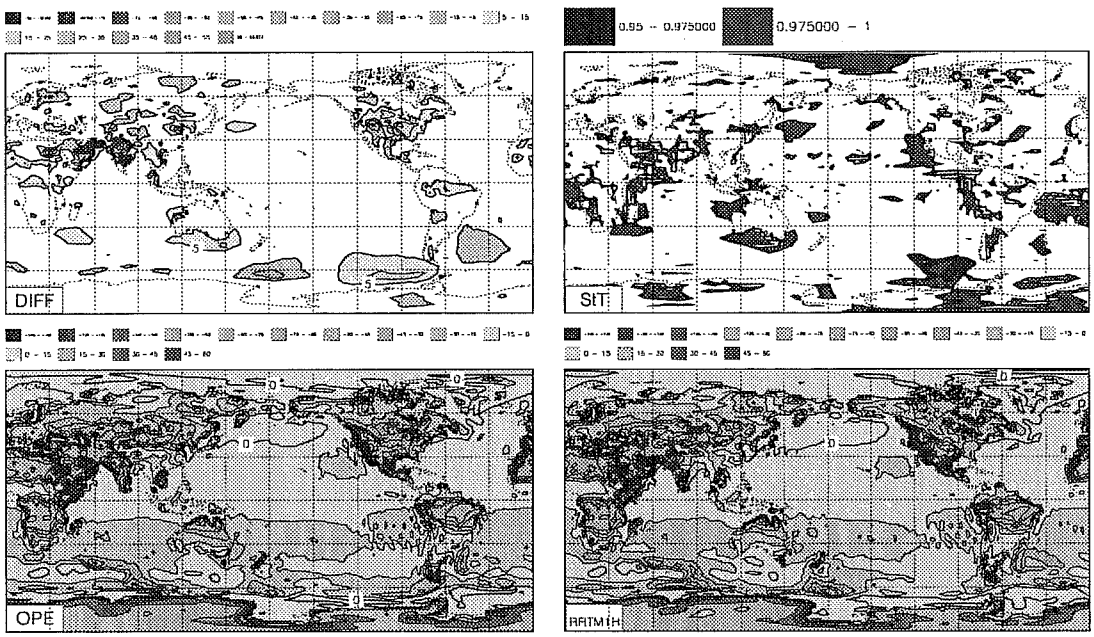

Figure 25: As in Figure 9, but for the surface sensible heat flux. Global means are: Control -17.7 W/m^2, RRTM -17.2 W/m^2, difference RRTM-Control -0.5 W/m^2.

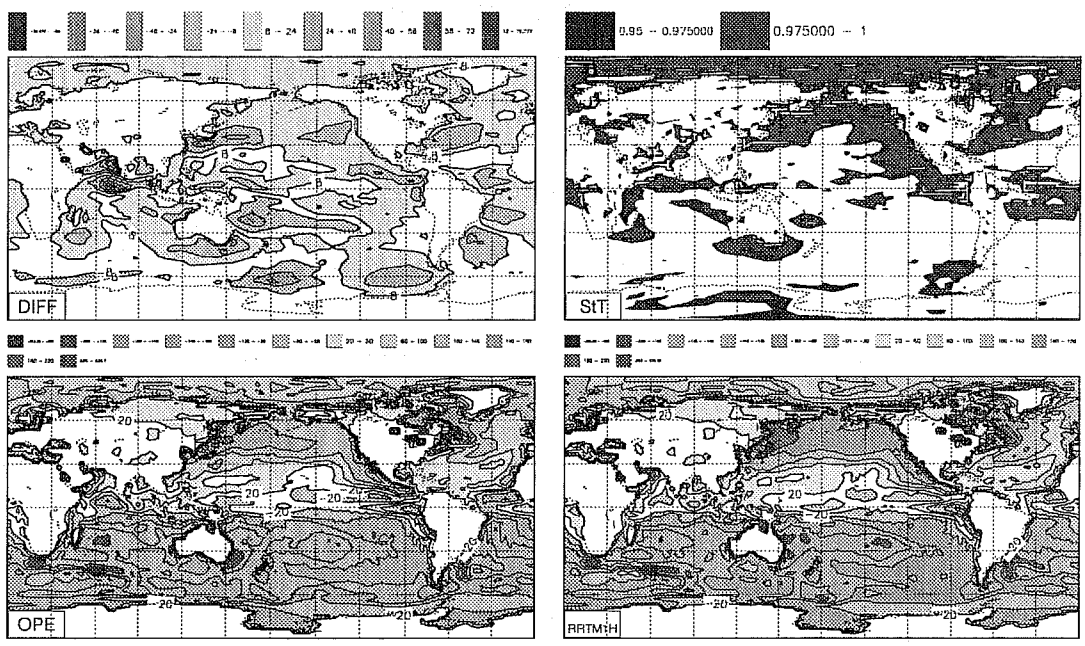

Figure 26: As in Figure 9, but for the net heat flux at the surface. Global means are: Control -19.8 W/m^2, RRTM -12.7 W/m^2, difference RRTM-Control 7.0 W/m^2.

As seen in Figure 27, the temperature follows by and large the changes in radiative heating rates. RRTM produces a warmer lower troposphere and a cooler high troposphere and stratosphere, a signal statistically significant over most heights and latitudes, except the lower troposphere of the Southern hemisphere. As seen in Figure 28, for the relative humidity, the warmer temperature of the lower troposphere and the reduced latent heat flux gives a drier lower troposphere, which explains the reduced cloudiness in the low to mid-levels. However, only the upper atmosphere signal seems statistically significant. For heights above the 300 hPa level in the Northern hemisphere and in the Southern hemisphere poleward of 40 ^{o}S, the increased relative humidity follows the decrease in temperature.

Through the thermal wind argument, the changes in temperature (Fig. 27) partly explain the changes in zonal wind (Fig. 29). The larger pole-equator temperature gradient in the winter hemisphere, at 200 hPa and above, translates into slighly stronger zonal wind. Also noticeable are the stronger easterlies which extend from 850 to 100 hPa in the equatorial area, and the decrease in the meridional wind between 300 and 200 hPa (Fig. 30). As seen in Figure 27, the increased vertical gradient of temperature in the tropics destabilizes the atmosphere and impacts the vertical velocity (Fig. 31), with larger upward velocity in the ITCZ (about 5 ^{o}N) and larger subsidence on both sides of it (30 ^{o}N and 15 ^{o}S)

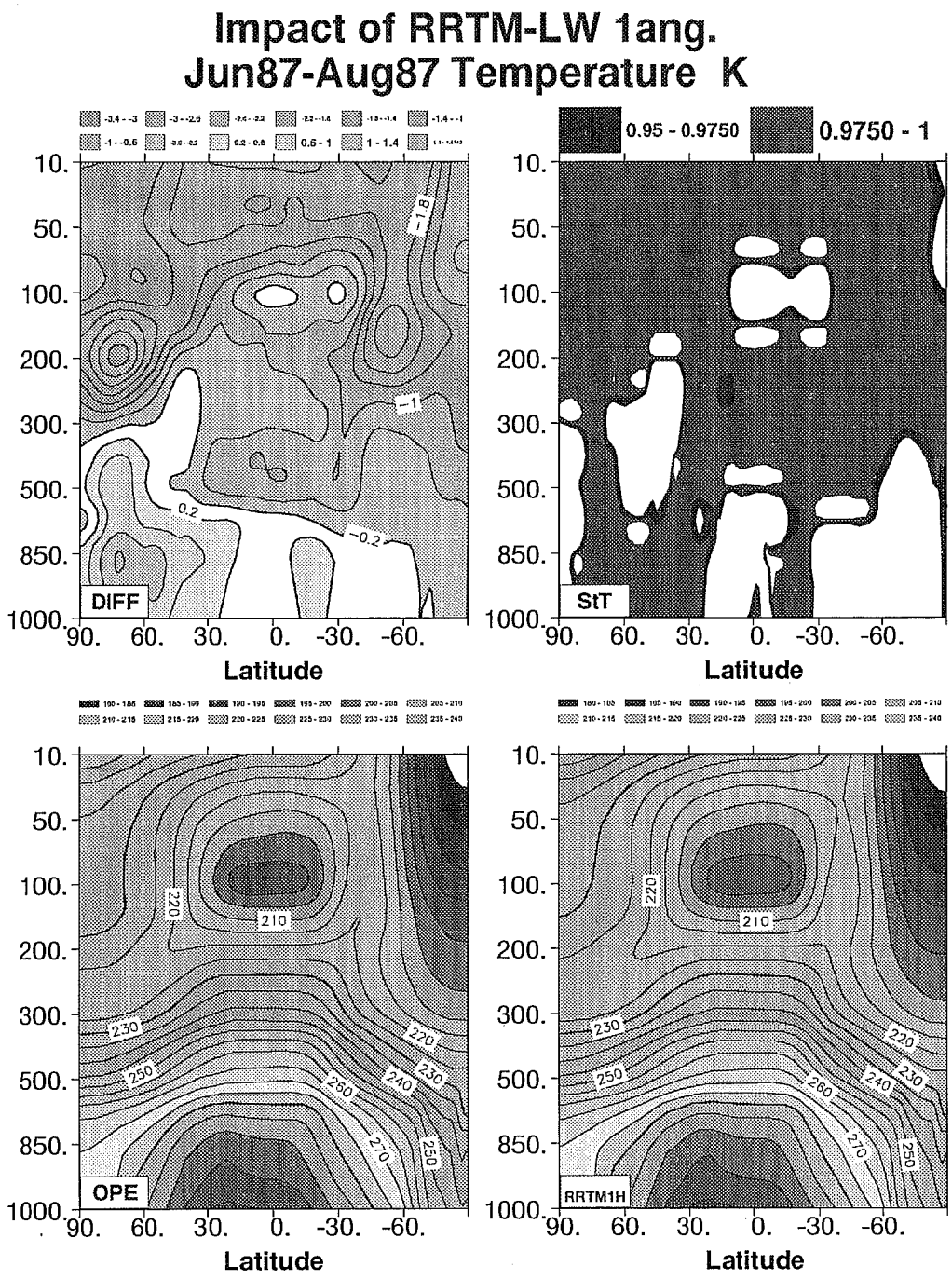

Figure 27: The vertical and latitudinal distribution of the zonally averaged temperature averaged over JJA87. Bottom left panel is Control, bottom right panel is RRTM, top left is difference RRTM-Control, top right panel is the result of Student's t-test performed on the two sets of zonal means.

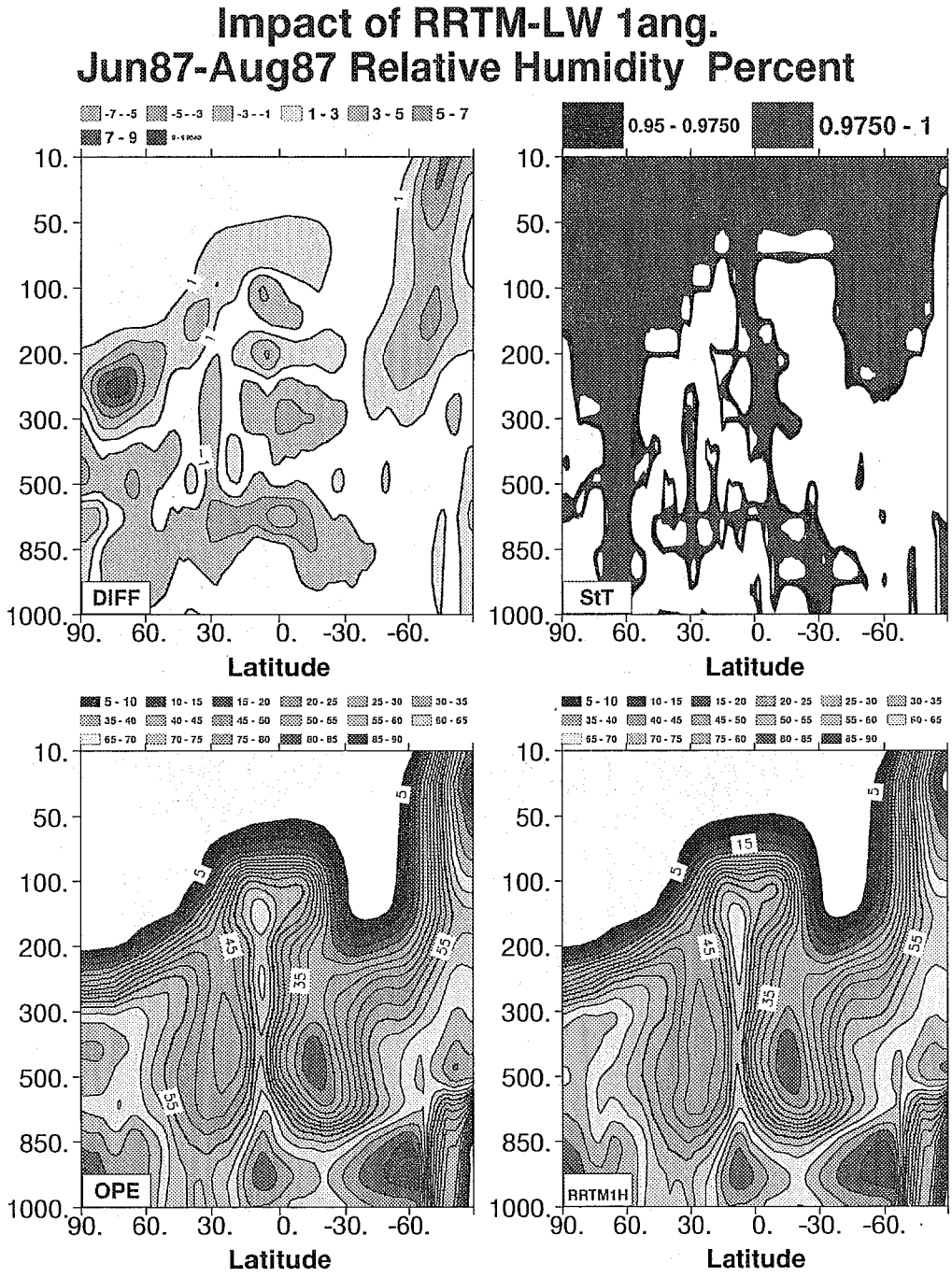

Figure 28: As in Figure 27, but for the relative humidity.

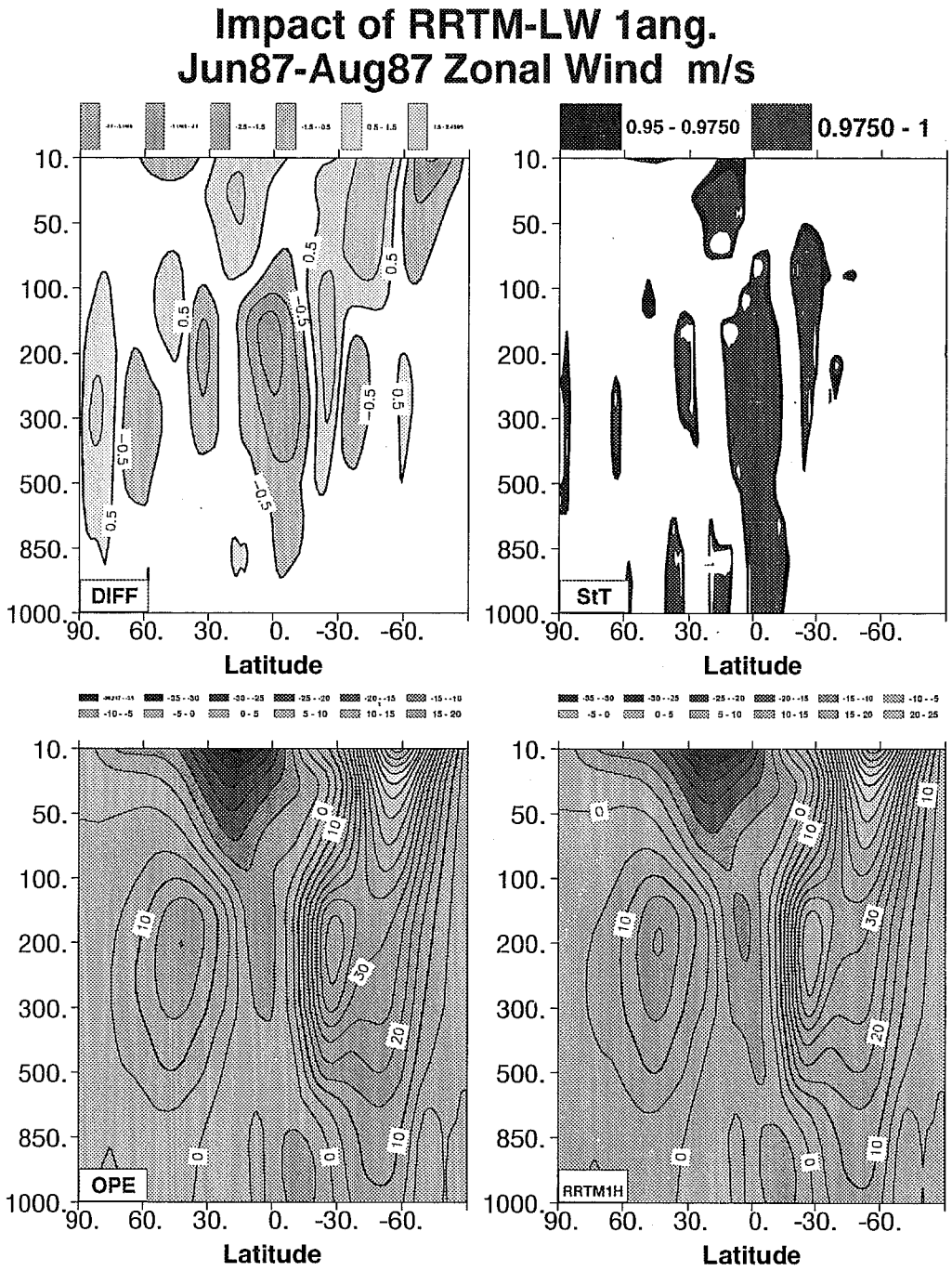

Figure 29: As in Figure 27, but for the zonal component of the wind.

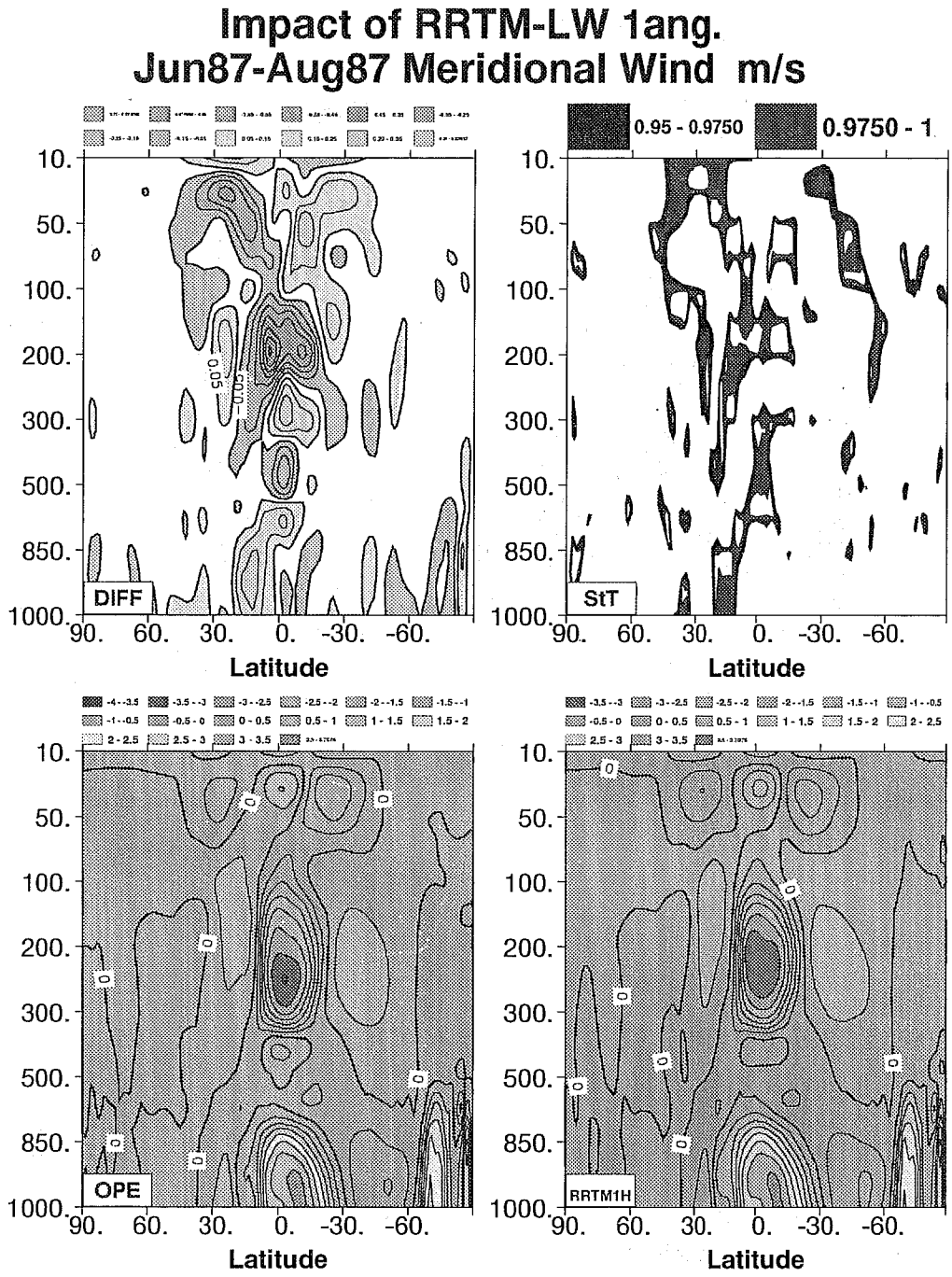

Figure 30: As in Figure 27, but for the meridional component of the wind.

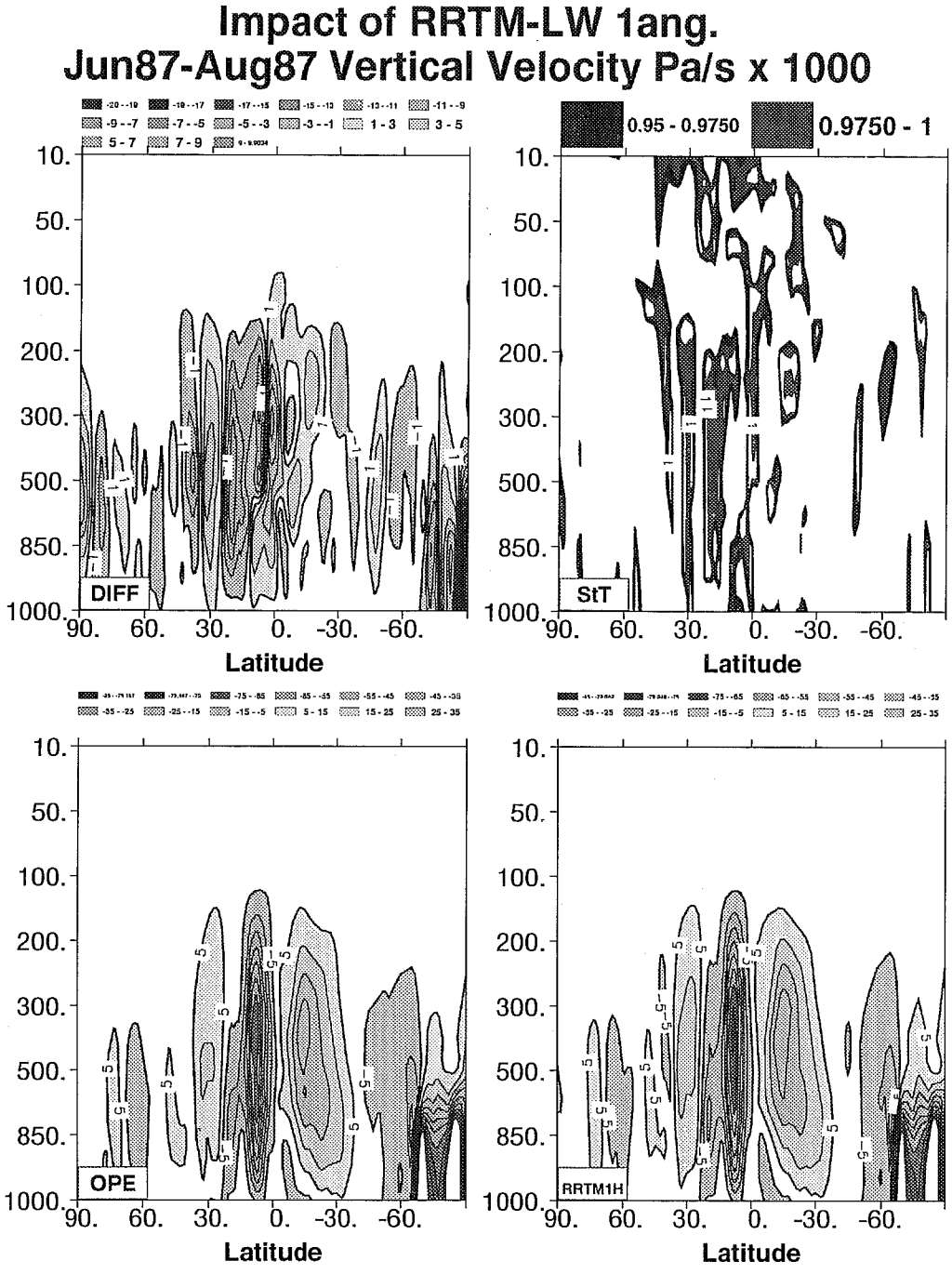

Figure 31: As in Figure 27, but for the vertical velocity.

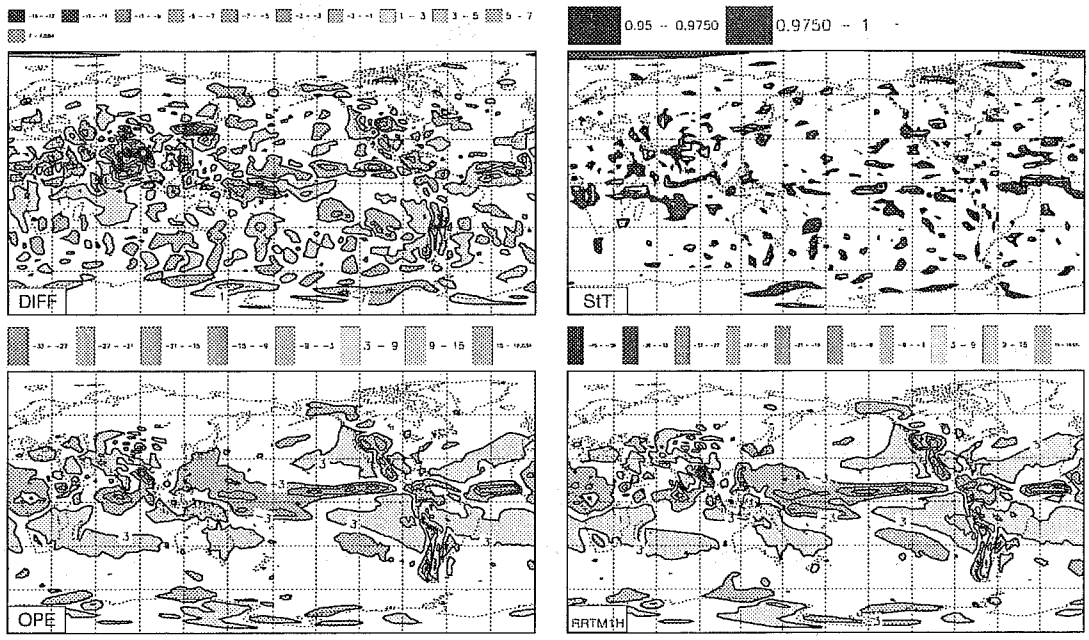

Figure 32: The vertical velocity at 500 hPa (Pa/s x 100).

The impact on the precipitation follows the increase in vertical velocity in the equatorial zone (Figs. 31 and 32). There is a large increase in convective precipitation (Fig. 33) together with a decrease in large-scale precipitation (Fig. 34) showing that a large part of the precipitation comes from the decreased stability of the higher equatorial layers. It is worth noting that, on a global average basis, the increase in total precipitation from 3.20 to 3.21 mm/day is relatively small, and appears more like a transfer from large-scale to convective precipitation ((Fig. 35).

Finally, the increase in net total radiation at the surface (Figs. 12 for LW and 23 for SW) translates into larger surface skin temperature (Fig. 36) over most of the continents, the only exception being over the United States.

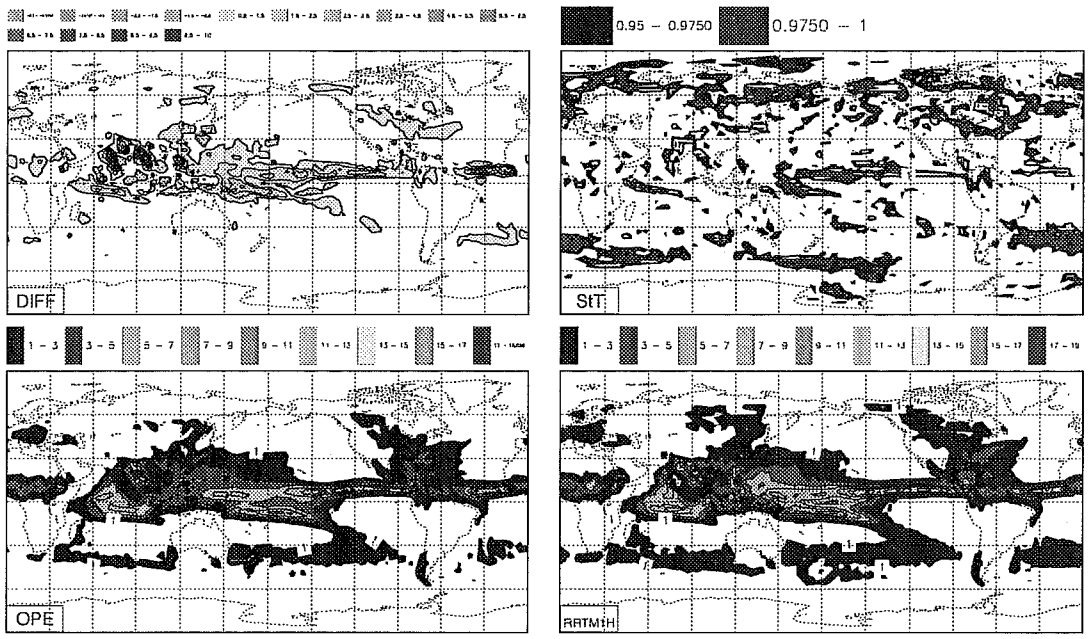

Figure 33: The convective precipitation averaged over the last three months of the integrations. Global means are: Control 1.23 mm/day, RRTM 1.48 mm/day, difference RRTM-Control is 0.25 mm/day.

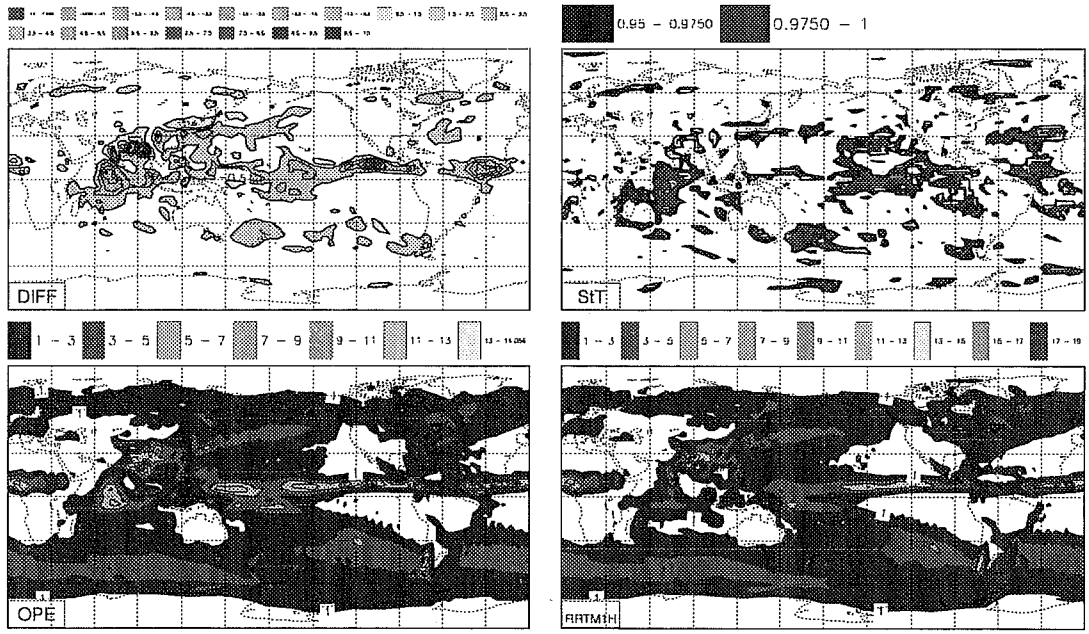

Figure 34: As in Figure 33, but for the large-scale precipitation. Global means are: Control 1.96 mm/day, RRTM 1.72 mm/day, difference RRTM-Control -0.24 mm/day.

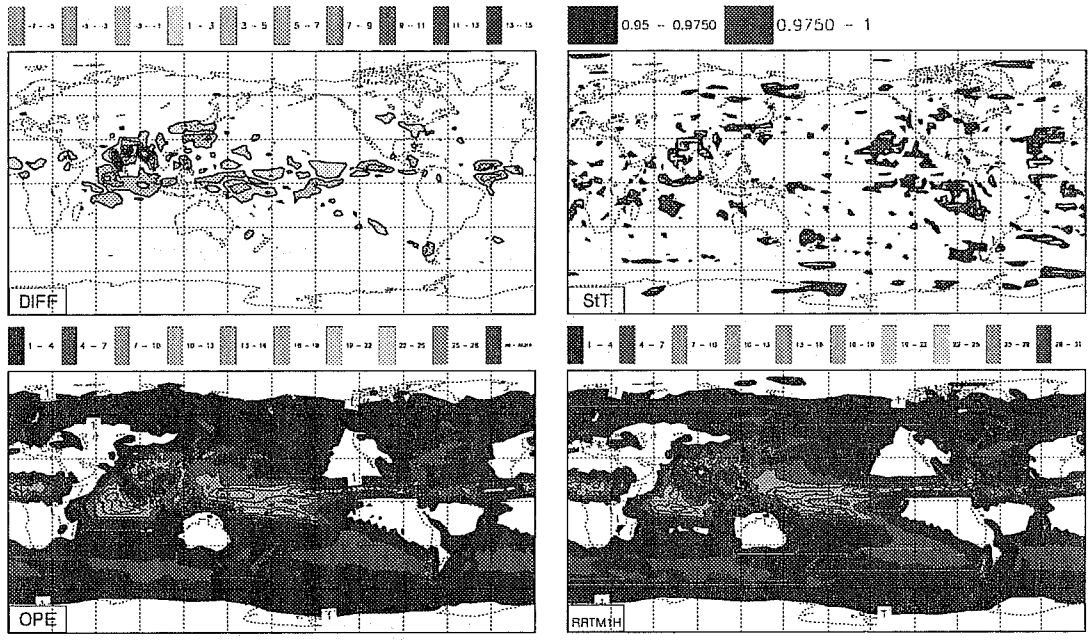

Figure 35: As in Figure 33, but for the total precipitation. Global means are: Control 3.19 mm/day, RRTM 3.20 mm/day, difference RRTM-Control 0.01 mm/day.

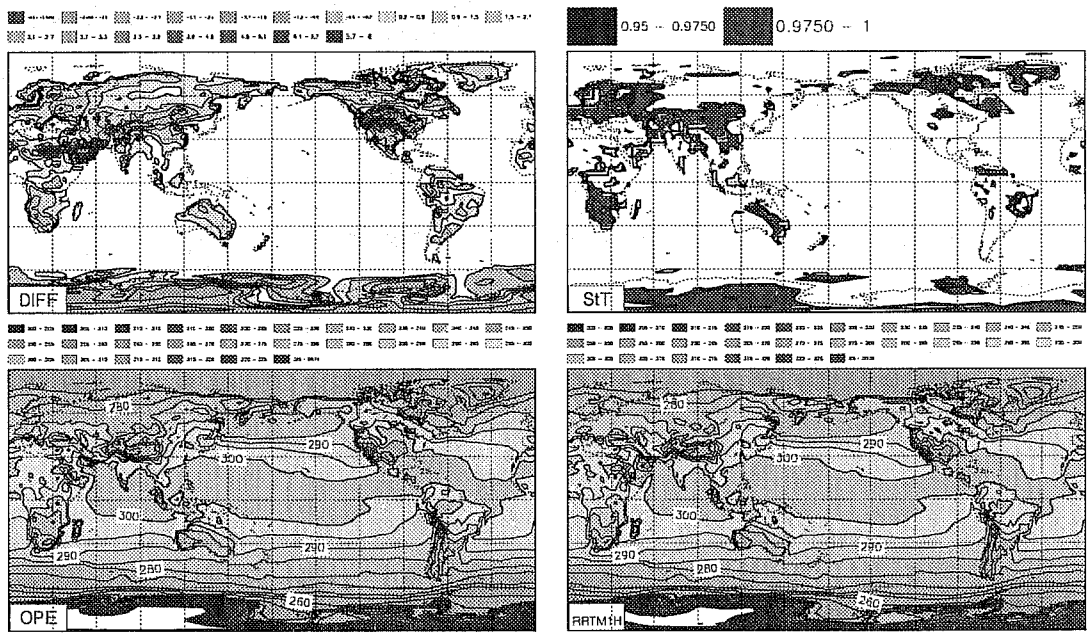

Figure 36: The geographical distribution of the surface skin temperature (K). The variation of the sea surface temperature is similarly prescribed in both sets of experiments. Global means are: Control 288.53 K, RRTM 288.78 K, difference RRTM-Control 0.24 K.

3.3 Winter results

Most of the signal seen in summer also appears in winter. For example, Figures 37 and 38 respectively present the outgoing LW radiation and net LW radiation at the surface, averaged over the last 3 months of the 4-month winter simulations starting on 1 November 1987. The pattern of reduction in OLR and of increase in surface downward LW radiation over most of subtropics, where clear-sky or low-level clouds prevail, is consistent with what is seen in summer conditions (Figs. 11 and 12). The increase in land surface temperature, seen in Figure 39 over most of the Northern continents, is linked to the increased opacity of the atmosphere brought by RRTM, and is a positive step towards the reduction of one of the ECMWF long-running systematic errors. As in summer, RRTM reduces the overall cloud cover (Fig. 40) specifically through a reduction of both the high and middle level cloudiness (not shown). This translates into an increase in surface net SW radiation and in net surface heat flux (not shown).

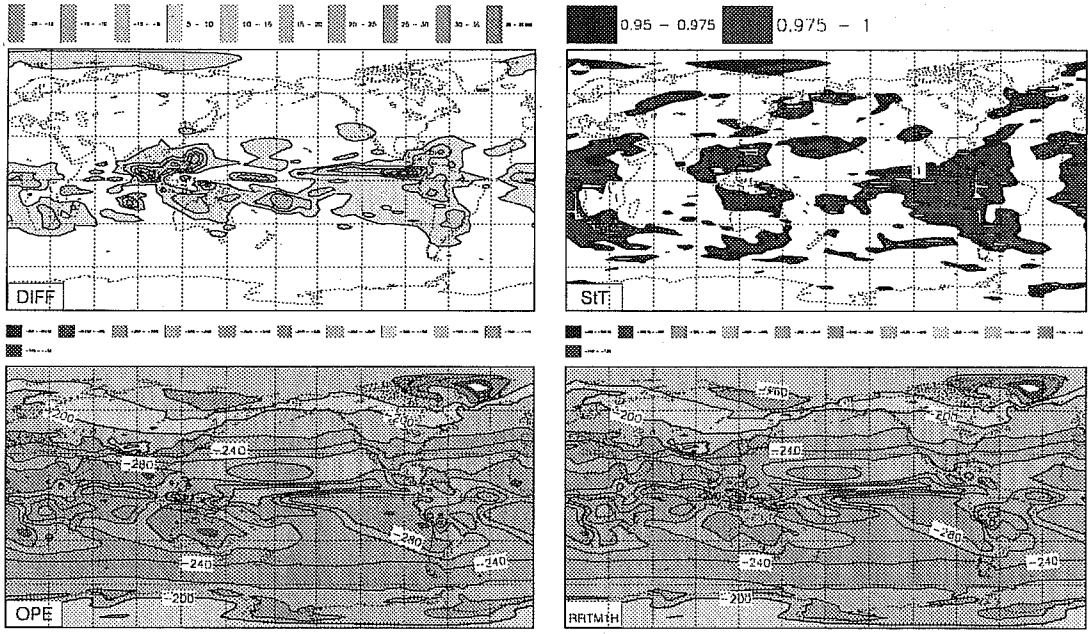

Figure 37: The outgoing LW radiation at the top of the atmosphere averaged over 91 days between 871201 00Z and 880229 24Z. Global means are: Control -244.6 W/m^2, RRTM -241.8 W/m^2, difference RRTM-Control 2.9 W/m^2.

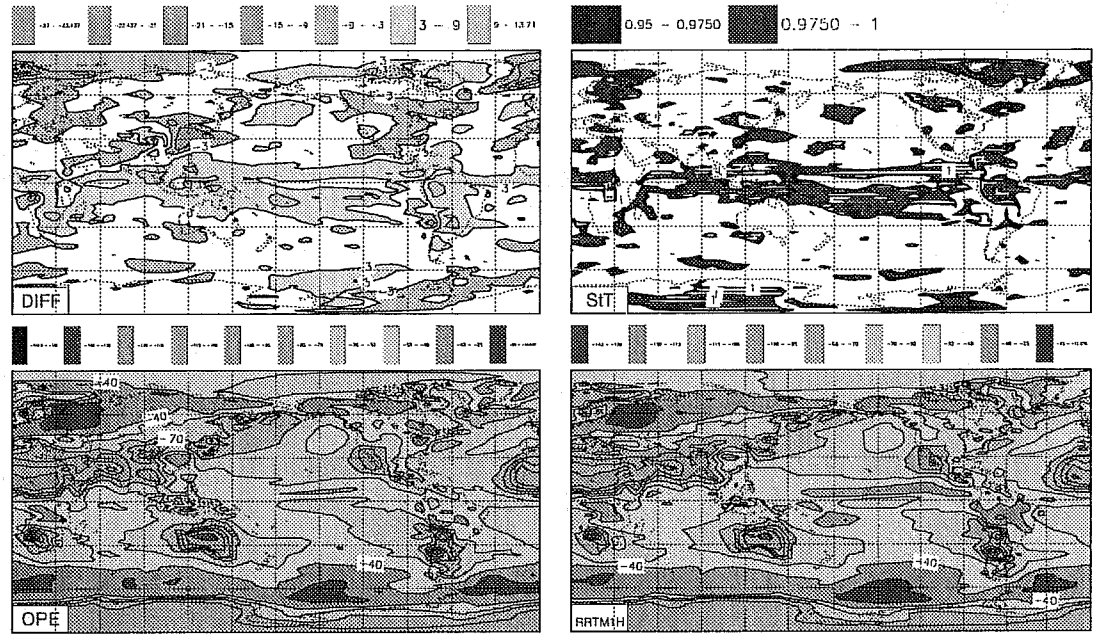

Figure 38: As in Figure 37, but for the surface net LW radiation. Global means are: Control -57.9 W/m^2, RRTM -57.1 W/m^2, difference RRTM - Control 0.8 W/m^2.

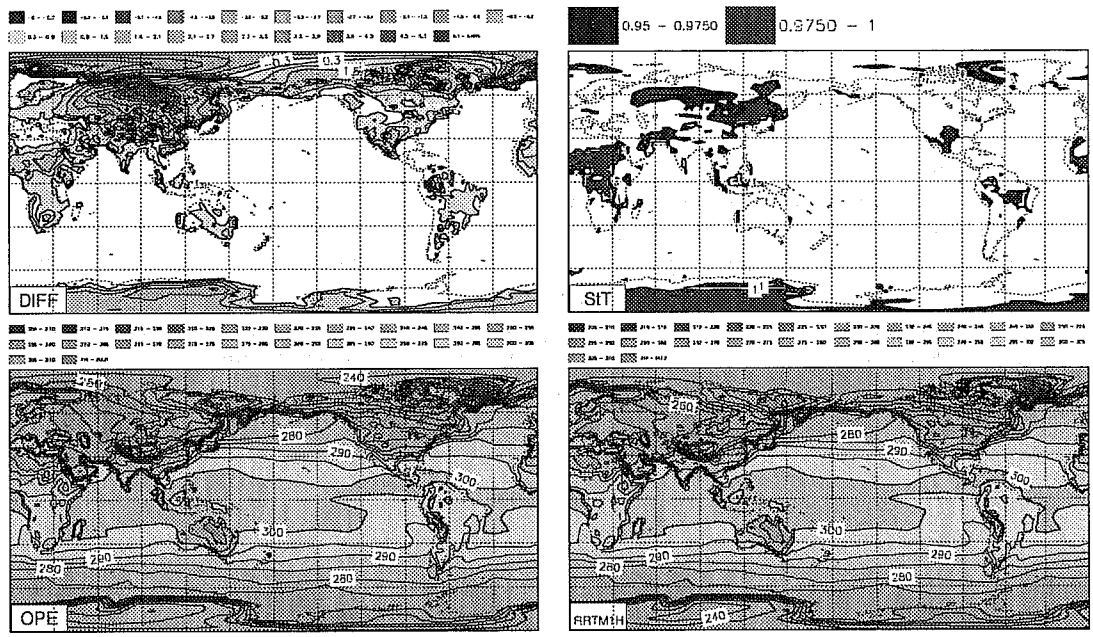

Figure 39: As in Figure 37, but for the surface skin temperature in the winter simulations. Global means are: Control 285.70 K, RRTM 285.94 K, difference RRTM-Control 0.25 K.

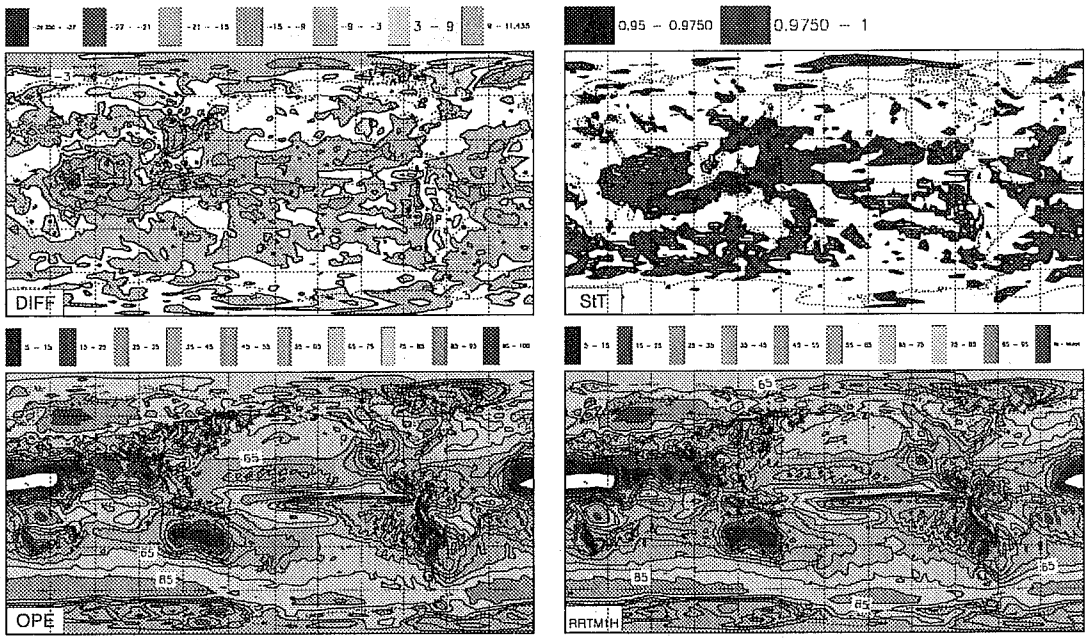

Figure 40: As in Figure 37, but for the total cloudiness. Global means are: Control 59.2 percent, RRTM 54.9 percent, difference RRTM-Control -4.3 percent.

3.4 Energetics

In a weather forecast environment, one of the main questions is whether an increase in the cooling (of radiative or other origin) of the higher troposphere will translate into an increase in the level of eddy kinetic energy, a fact usually linked with a deterioration of the forecast quality. As can be seen in the Lorenz energy diagrams presented in Figure 41 for the Northern hemisphere winter and in Figure 42 for the Southern hemisphere winter, in the 4-month long simulations, the eddy kinetic energy averaged over the depth of the atmosphere and the three last months of the simulations remains shows no particular sign of an increase. This is confirmed by the time history of the eddy kinetic energy over the length of the simulations (not shown).

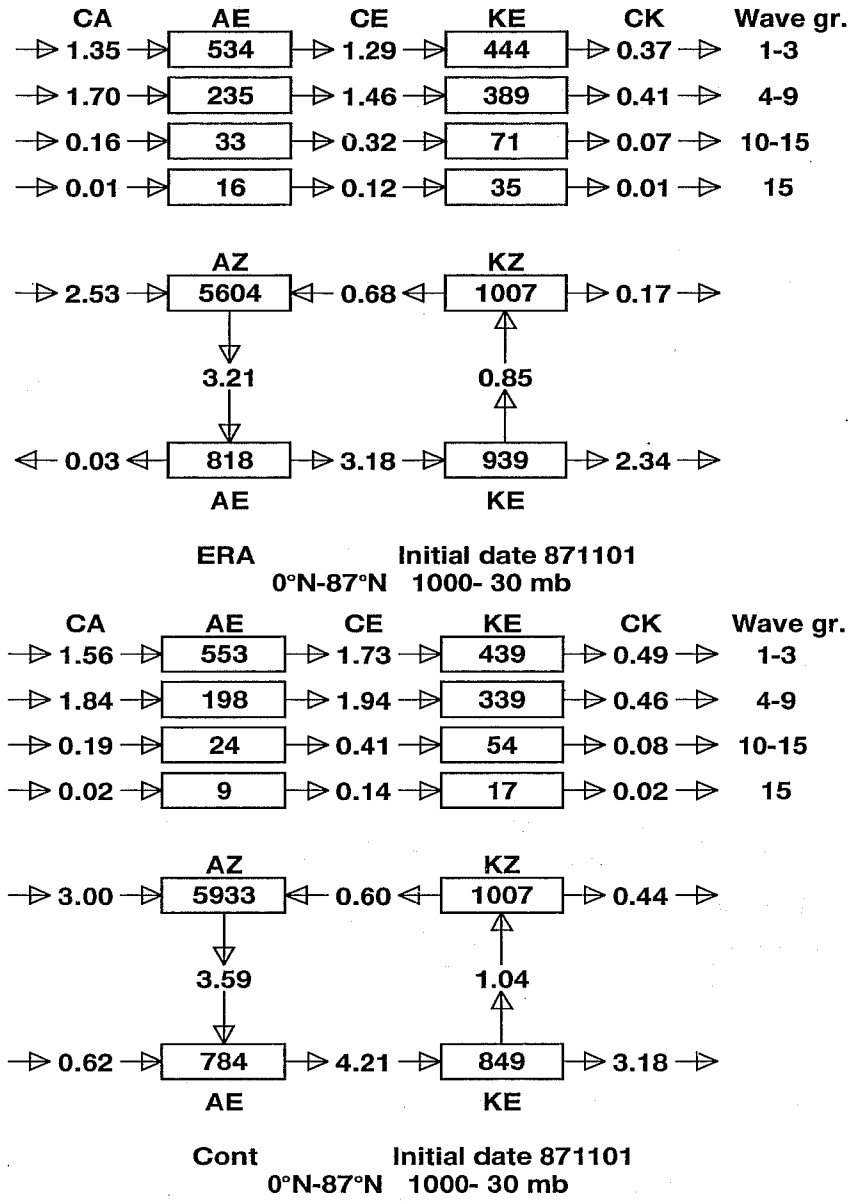

Figure 41: Lorenz energy diagrams for the Northern hemiosphere winter as analysed by ERA (first panel), and simulated by the ECMWF model including the operational (second panel) and RRTM LW radiation schemes (third panel).

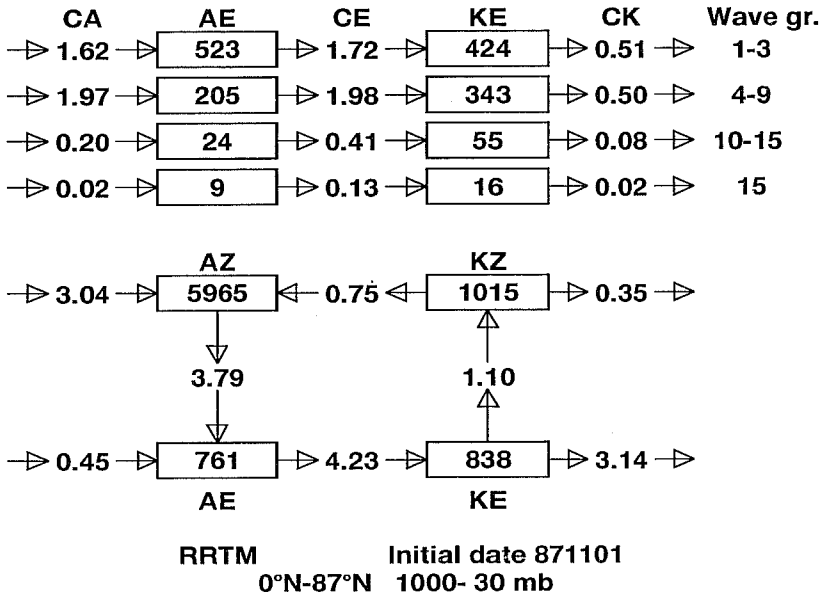

Figure 41: third panel

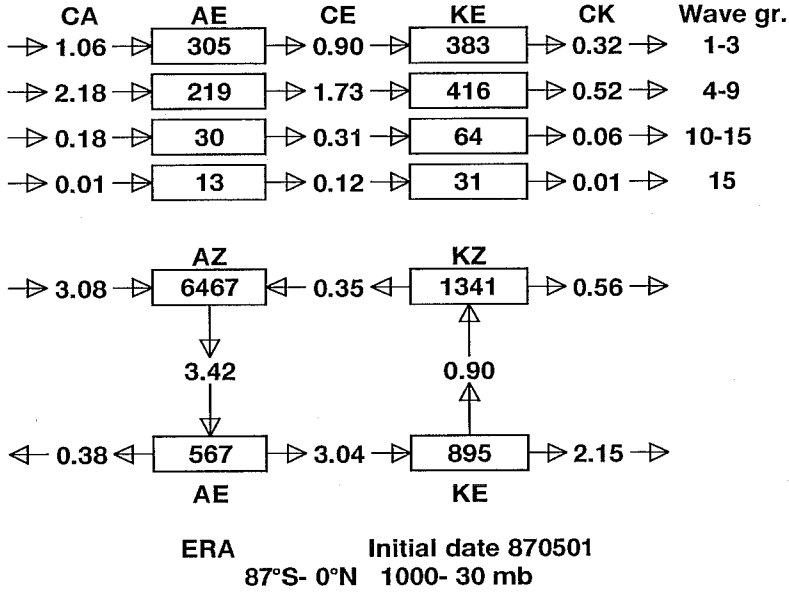

Figure 42: As in Figure 41, but for the energy cycle over the Southern hemisphere winter.

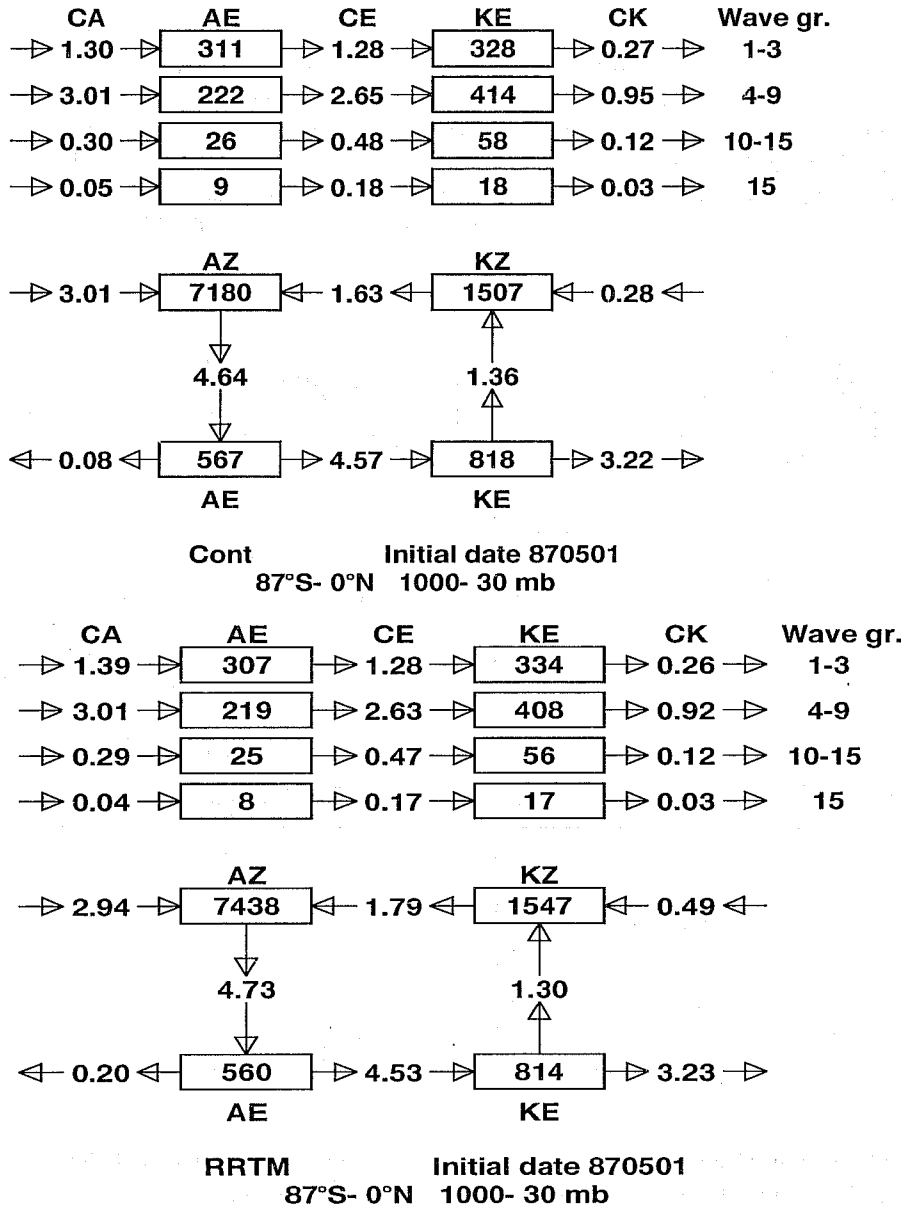

Figure 42: continued.

4. Forecast results

Here we compare the objective scores for two sets of 12 T213 L31 experiments starting from the 15th of each month between 15 April 1996 and 15 March 1997. Figures 43 and 44 present the anomaly correlation and the root mean square error of the geopotential at 1000 and 500 hPa for both the Northern and Southern hemispheres. It can be seen that RRTM has quite a small impact on this score. As already noted in the section 3.4 for the seasonal runs, it is of interest that the initial increased cooling in the high troposphere does not readily translate into a deterioration of these objective scores, via an increased temperature bias, and an increase in the kinetic energy of the model.

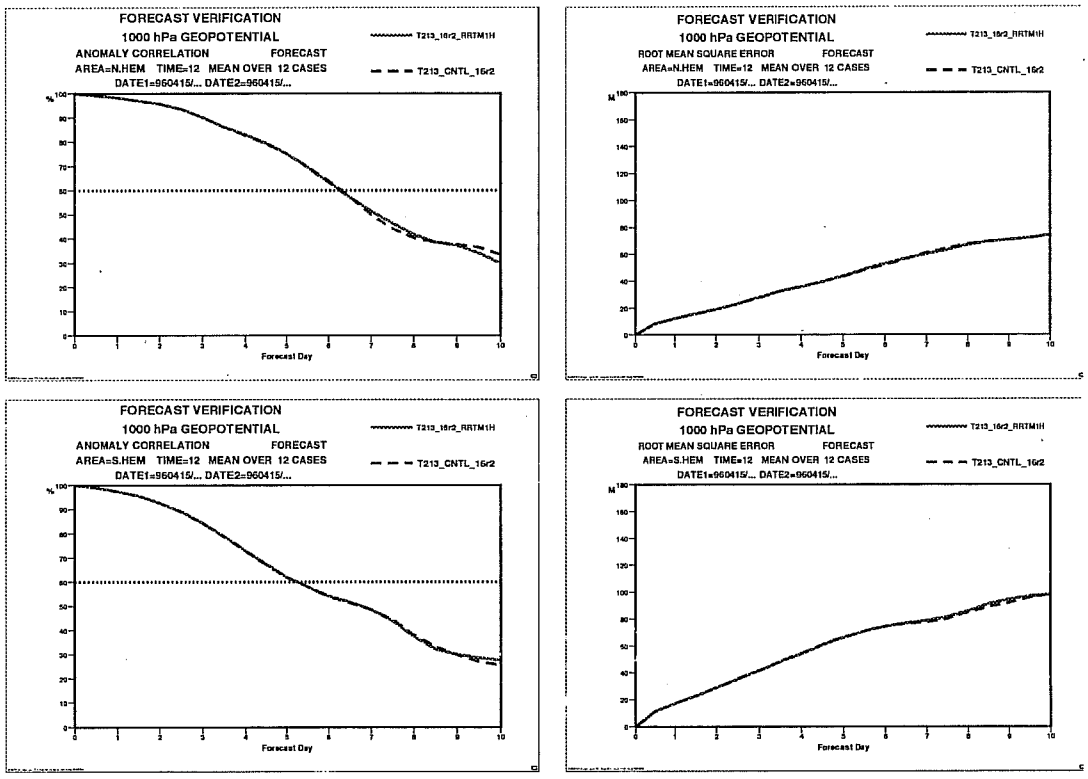

Figure 43: The anomaly correlation and root mean square error of geopotential at 1000 hPa from sets of 12 T213 simulations, from 960415 to 970315, with the operational radiation scheme (CNTL) and RRTM.

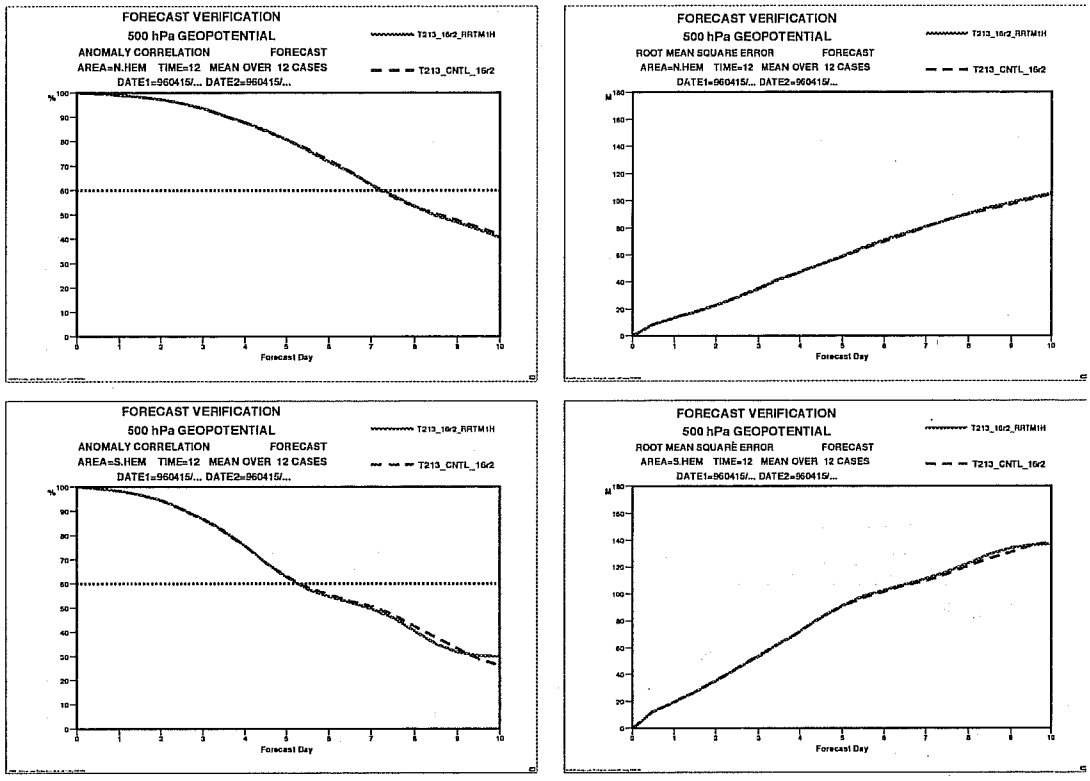

Figure 44: As in Figure 43, but for the anomaly correlation and root mean square error of geopotential at 500 hPa.

Compared to the impact on anomaly correlation and r.m.s. error of geopotential, the impact on temperature is much bigger, as can be seen from Figures 45 and 46, which shows a comparison of the temperature mean error at 850, 500, 200 and 50 hPa, for both hemispheres and in the tropics. At 850 hPa, the enhanced greenhouse effect of RRTM prevents the cooling seen with the operational scheme, where the opposite holds at 500 hPa. Higher up, the impact of RRTM is largely positive with smaller departure from the analyzed temperature than the operational scheme produces. This is particularly the case at 50 hPa for both hemispheres, whereas in the tropics at this height RRTM has a tendency to cool more. Overall, the various signals indicate a rather strong interaction with the cloudiness. In the tropics, the impact of RRTM on the winds, as seen in Figure 47 in a comparison of the r.m.s. error of the wind at 850, 500, 200 and 50 hPa is almost non-existent.

As seen from the previous scores, the impact on the forecast quality appears small. This is confirmed by the impact on individual forecasts, as seen from the scatter of the anomaly correlation of geopotential at 500 hPa, presented in Figures 48 to 49 for the Northern and Southern hemispheres, and in Figure 50 over the European region, respectively.

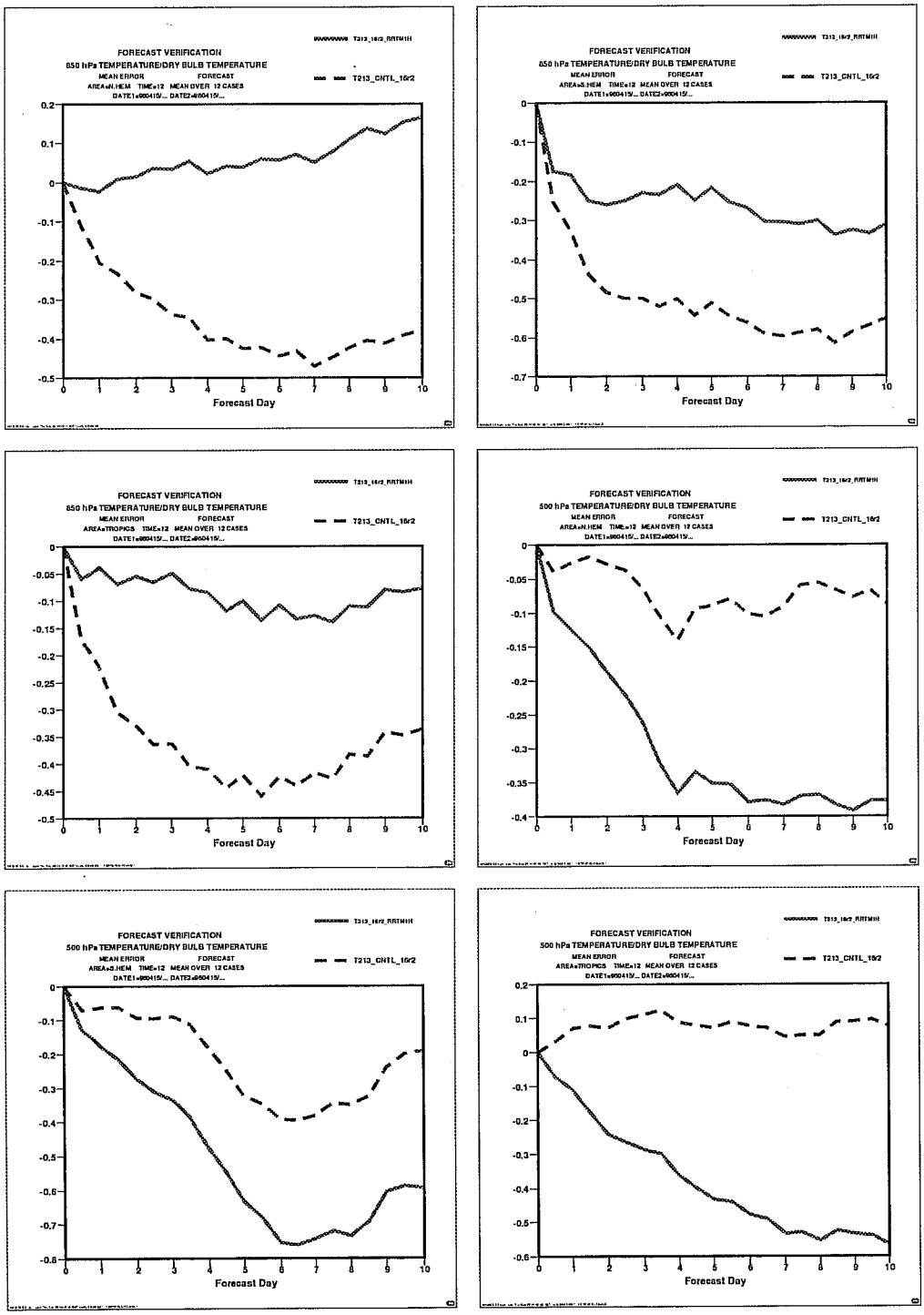

Figure 45: The mean temperature error at 850 and 500 hPa over the Northern hemisphere, Southern hemisphere and tropical area for the same sets of experiments.

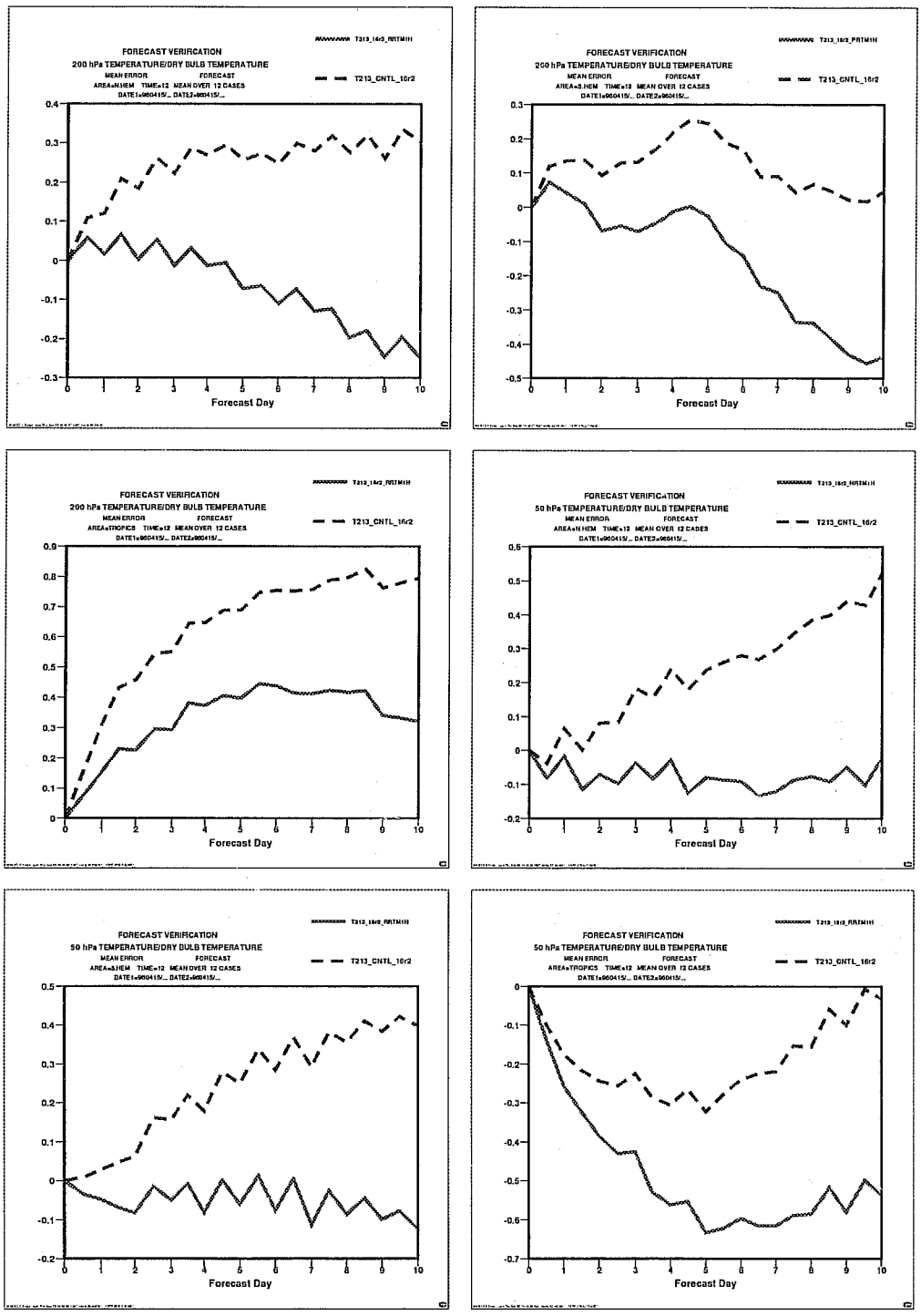

Figure 46: As in Figure 45, but for the mean temperature error at 200 and 50 hPa.

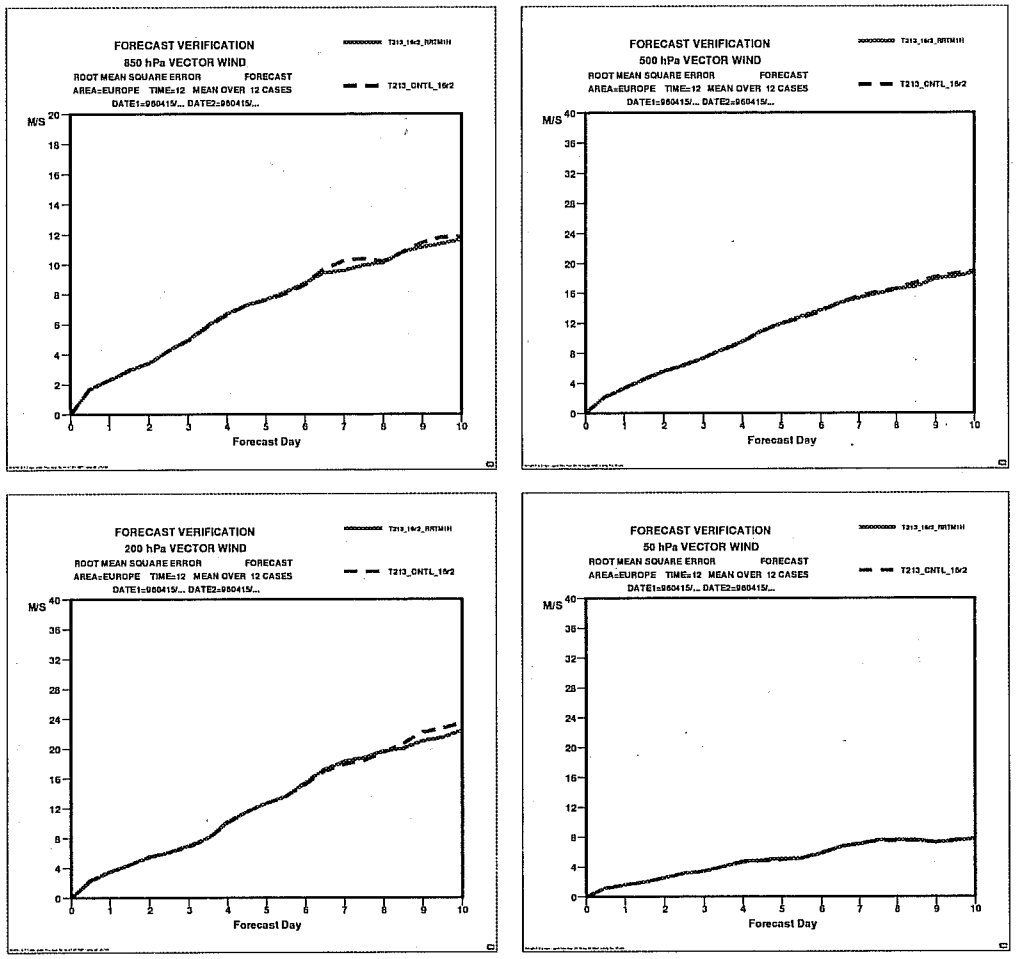

Figure 47: The root mean square error on the tropical wind at 850, 500, 200, and 50 hPa for the same sets of experiments.

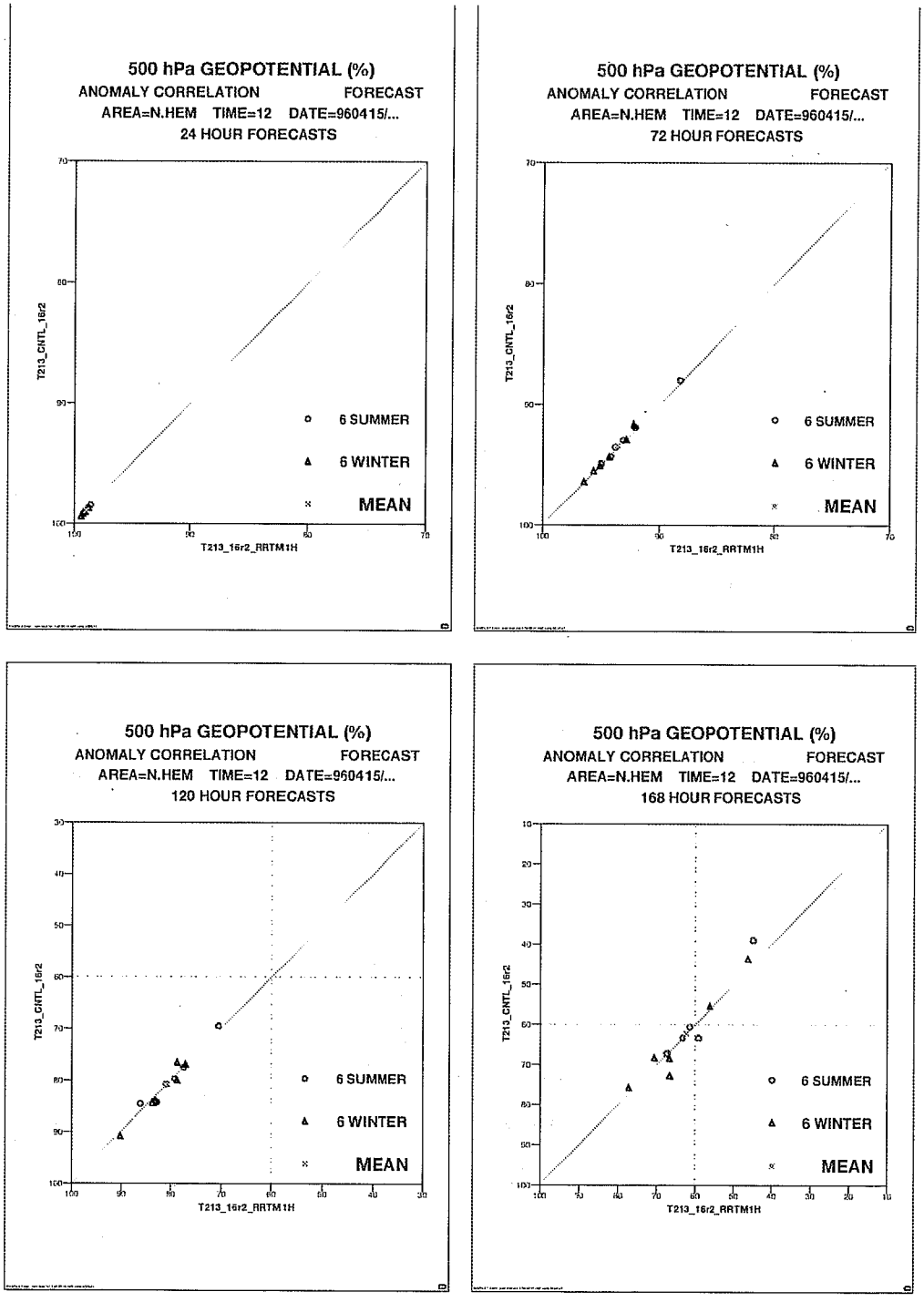

Figure 48: The anomaly correlation of the geopotential at 500 hPa over the Northern hemisphere after 24, 72, 120 and 168 hours of forecast. Symbols over the diagonal denote a positive impact of RRTM relative to the operational LW radiation scheme.

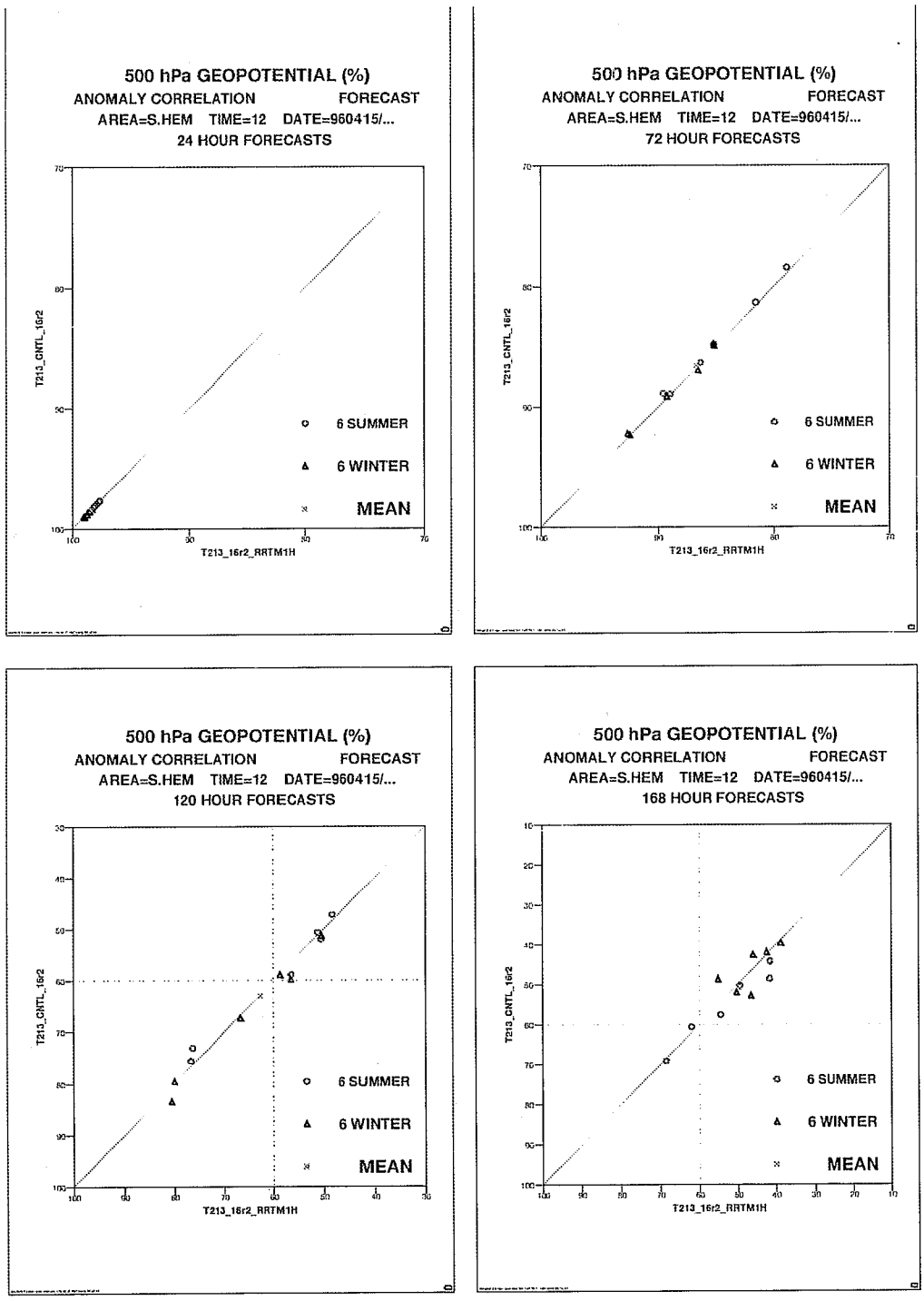

Figure 49: As in Figure 48, but for the anomaly correlation over the Southern hemisphere.

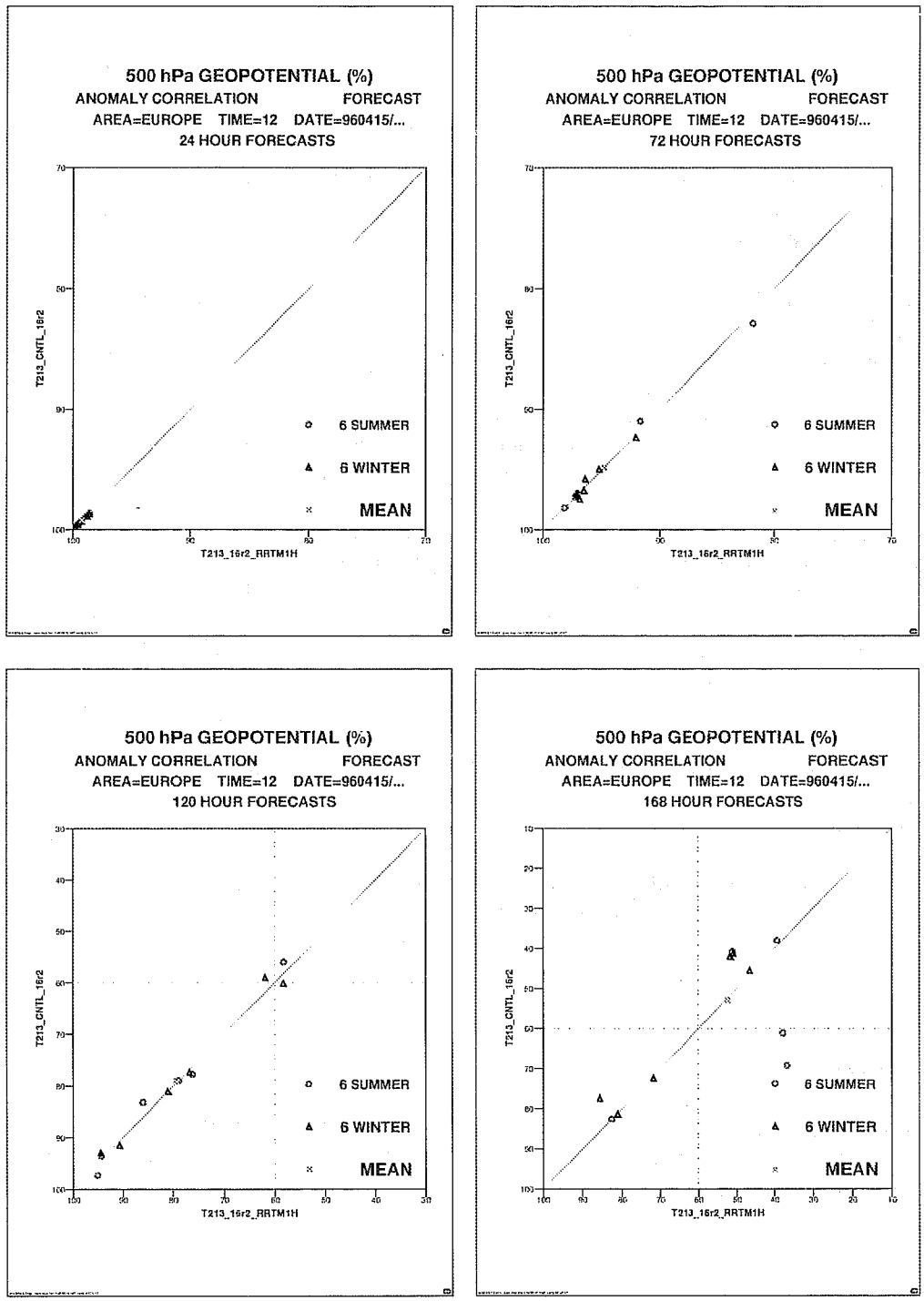

Figure 50: As in Figure 48, but for the anomaly correlation over the European area.

5. Discussion and conclusions

The Rapid Radiation Transfer Model of Mlawer et al. (1997) has been introduced into the ECMWF model. This LW radiation scheme, developed for use in GCMs, directly follows from a line-by-line model (LBLRTM), which has been and is still validated over a large sample of atmospheric conditions as part of the ARM program. In the configuration used for this study, RRTM offers a remarkably good trade-off between computational efficiency and accuracy of results. While heavily dependent on the line-by-line model to which it was fitted, RRTM remains quite flexible in terms of cloud specifications, i.e., whether cloud scattering is included or not, how the cloud optical properties are defined, what cloud overlap is assumed.

The impact of RRTM was compared to that of the current operational LW radiation scheme (as of cycle 16), in both T63 seasonal simulations and T213 10-day forecasts. Both winter and summer seasonal simulations show an improvement on the systematic errors in the LW fields, namely a decreased outgoing longwave radiation, and an increased downward longwave radiation at the surface. As previously documented in comparison of results with the operational LW scheme with ERBE measurements for OLR, and with station measurements for surface LW radiation, both types of errors occur at all ranges, in first-guess 6-hour forecasts used for analysis, 10-day forecasts, and long simulations of seasonal scale and beyond. The better results with RRTM, reported here for 10-day forecasts and seasonal runs, stem mainly from the initial improvement in clear-sky radiation, due to the improved representation of the water vapour absorption. Accompanying the change in LW radiation transfer, a number of other aspects of the model are modified, sometimes strongly as, for example, the balance between convective and large scale precipitation in the tropics, or the overall decrease in cloudiness at most levels, or the surface net energy budget over the ocean.

With respect to the increased LW opacity of the atmosphere with RRTM, it is particularly worth noting that the initial increased longwave cooling of the high troposphere that accompanied the changes in fluxes does not readily translate into a large increase in temperature bias in long simulations, nor to a degradation of the objective scores via an increase in the eddy kinetic energy of the model in 10-day forecasts.

Inasmuch as the results reported here were obtained with the operational model without any tuning other than the change of LW scheme, further improvements might be expected from a better adjustment of some of the other physical parametrizations.

Acknowledgments

All figures related to the energy cycle in Section 3.4 were kindly provided by Cedo Brankovic. Anthony Hollingsworth, Martin Miller and Anton Beljaars are thanked for reading and commenting on draft versions of this report.

References

Brankovic, C., T.N. Palmer, and L. Ferranti, 1994: Predictability of seasonal atmospheric variations. J. Climate, 7, 217–237.

Clough, S.A., F.X. Kneizys, and R.W. Davies, 1989: Line shape and the water vapor continuum. Atmospheric Research, 23, 229-241.

Clough, S.A., M.I. Iacono, and J.-L. Moncet, 1992: Line-by-line calculations of atmospheric fluxes and cooling rates: Application to water vapor. J. Geophys. Res., 97D, 15761-15786.

Clough, S.A., and M.I. Iacono, 1995: Line-by-line calculation of atmospheric fluxes and cooling rates, 2, Application to carbon dioxide, ozone, methane, nitrous oxide and the halocarbons. J. Geophys. Res., 100D, 16519-16536.

ECMWF Forecast Model, Research Manual 3, Physical Parameterisation, 3rd Ed., July 1991.

Fouquart, Y., 1987: Radiative transfer in climate models. NATO Advanced Study Institute on Physically-Based Modelling and Simulation of Climate and Climatic Changes. Erice, Sicily, 11-23 May 1986. M.E. Schlesinger, Ed., Kluwer Academic Publishers, 223-284.

Fouquart, Y., and B. Bonnel, 1980: Computations of solar heating of the earth's atmosphere: a new parameterization. Beitr. Phys. Atmosph., 53, 35-62.

Iacono, M.J., and S.A. Clough, 1996: Application of infrared interferometer spectrometer clear sky spectral radiance to investigations of climate variability. J. Geophys. Res., 101D, 29439-29460.

Mlawer, E.J., S.J. Taubman, P.D. Brown, M.J. Iacono, and S.A. Clough, 1997: Radiative transfer for inhomogeneous atmospheres: RRTM, a validated correlated-k model for the longwave. J. Geophys. Res., 102D, 16,663-16,682.

Morcrette, J.-J., 1989: Description of the radiation scheme in the ECMWF model. ECMWF Research Department Tech. Memo. No. 165, 26 pp.

Morcrette, J.-J., 1991: Radiation and cloud radiative properties in the ECMWF operational weather forecast model. J. Geophys. Res., 96D, 9121-9132.

Morcrette, J.-J., 1993: Revision of the clear-sky and cloud radiative properties in the ECMWF model. ECMWF Newsletter, 61, 3-14.

Morcrette, J.-J., and Y. Fouquart, 1985: On systematic errors in parametrized calculations of longwave radiation transfer. Quart.J.Roy.Meteor.Soc., 111, 691-708.

Morcrette, J.-J., L. Smith, and Y. Fouquart, 1986: Pressure and temperature dependence of the absorption in longwave radiation parameterizations. Beitr. Phys. Atmosph., 59, 455-469.

Roberts, R.E., J.E.A. Selby, and L.M. Biberman, 1976: Infrared continuum absorption by atmospheric water vapor in the 8-12 micron window. Appl. Opt., 15, 2085-2090.